

The fate of carbon in a mature forest under carbon dioxide enrichment

<https://doi.org/10.1038/s41586-020-2128-9>

Received: 10 July 2019

Accepted: 4 February 2020

Published online: 8 April 2020

 Check for updates

Mingkai Jiang¹✉, Belinda E. Medlyn¹✉, John E. Drake^{1,2}, Remko A. Duursma¹, Ian C. Anderson¹, Craig V. M. Barton¹, Matthias M. Boer¹, Yolima Carrillo¹, Laura Castañeda-Gómez¹, Luke Collins^{1,3,4}, Kristine Y. Crous¹, Martin G. De Kauwe^{5,6,7}, Bruna M. dos Santos^{8,9}, Kathryn M. Emmerson¹⁰, Sarah L. Facey¹, Andrew N. Gherlenda¹, Teresa E. Gimeno^{1,11,12}, Shun Hasegawa^{1,13}, Scott N. Johnson¹, Astrid Kännaste¹⁴, Catriona A. Macdonald¹, Kashif Mahmud^{1,15}, Ben D. Moore¹, Loïc Nazaries¹, Elizabeth H. J. Neilson^{8,9}, Uffe N. Nielsen¹, Ülo Niinemets¹⁴, Nam Jin Noh^{1,16}, Raúl Ochoa-Hueso^{1,17}, Varsha S. Pathare^{1,18}, Elise Pendall¹, Johanna Pihlblad¹, Juan Piñeiro^{1,19}, Jeff R. Powell¹, Sally A. Power¹, Peter B. Reich^{1,20}, Alexandre A. Renchon¹, Markus Riegler¹, Riikka Rinnan²¹, Paul D. Rymer¹, Roberto L. Salomón²², Brajesh K. Singh^{1,23}, Benjamin Smith^{1,24}, Mark G. Tjoelker¹, Jennifer K. M. Walker¹, Agnieszka Wujeska-Klause¹, Jinyan Yang¹, Sönke Zaehle²⁵ & David S. Ellsworth¹

Atmospheric carbon dioxide enrichment (eCO₂) can enhance plant carbon uptake and growth^{1–5}, thereby providing an important negative feedback to climate change by slowing the rate of increase of the atmospheric CO₂ concentration⁶. Although evidence gathered from young aggrading forests has generally indicated a strong CO₂ fertilization effect on biomass growth^{3–5}, it is unclear whether mature forests respond to eCO₂ in a similar way. In mature trees and forest stands^{7–10}, photosynthetic uptake has been found to increase under eCO₂ without any apparent accompanying growth response, leaving the fate of additional carbon fixed under eCO₂ unclear^{4,5,7–11}. Here using data from the first ecosystem-scale Free-Air CO₂ Enrichment (FACE) experiment in a mature forest, we constructed a comprehensive ecosystem carbon budget to track the fate of carbon as the forest responded to four years of eCO₂ exposure. We show that, although the eCO₂ treatment of +150 parts per million (+38 per cent) above ambient levels induced a 12 per cent (+247 grams of carbon per square metre per year) increase in carbon uptake through gross primary production, this additional carbon uptake did not lead to increased carbon sequestration at the ecosystem level. Instead, the majority of the extra carbon was emitted back into the atmosphere via several respiratory fluxes, with increased soil respiration alone accounting for half of the total uptake surplus. Our results call into question the predominant thinking that the capacity of forests to act as carbon sinks will be generally enhanced under eCO₂, and challenge the efficacy of climate mitigation strategies that rely on ubiquitous CO₂ fertilization as a driver of increased carbon sinks in global forests.

Globally, forests act as a large carbon sink, absorbing a substantial portion of the anthropogenic CO₂ emissions^{1,2}, an ecosystem service that has tremendous social and economic value. Whether mature forests will remain carbon sinks into the future is of critical importance for aspirations to limit climate warming to no more than 1.5 °C above pre-industrial levels¹³. FACE experiments provide an opportunity to determine the capacity of ecosystems to sequester carbon under the higher atmospheric CO₂ concentrations expected in the future^{3–5,7,8,10,11}. Evidence gathered from the four first-generation forest FACE experiments, which all measured responses of rapidly growing young forest plantations, has generally indicated a strong CO₂ fertilization effect on biomass growth^{3,4}. This CO₂ fertilization effect has been hypothesized

to be one of the largest drivers of the terrestrial carbon sink and its acceleration in recent decades¹⁴, potentially accounting for up to 60% of present-day terrestrial carbon sequestration². However, younger trees are generally more responsive to rising CO₂ than mature trees¹¹, potentially because nutrient limitation increases with stand age¹⁵. Thus, extrapolating evidence collected from these experiments on young trees may be argued to provide an upper limit on how much carbon can be stored by global forests under eCO₂ (ref. ¹⁶). Evidence from experiments with older trees on nutrient-poor soils suggests that although eCO₂ increases leaf photosynthesis to a similar degree as in young forests, stimulation of biomass growth and carbon storage may be lower or absent^{7–10}. Reconciling these conflicting observations

A list of affiliations appears at the end of the paper.

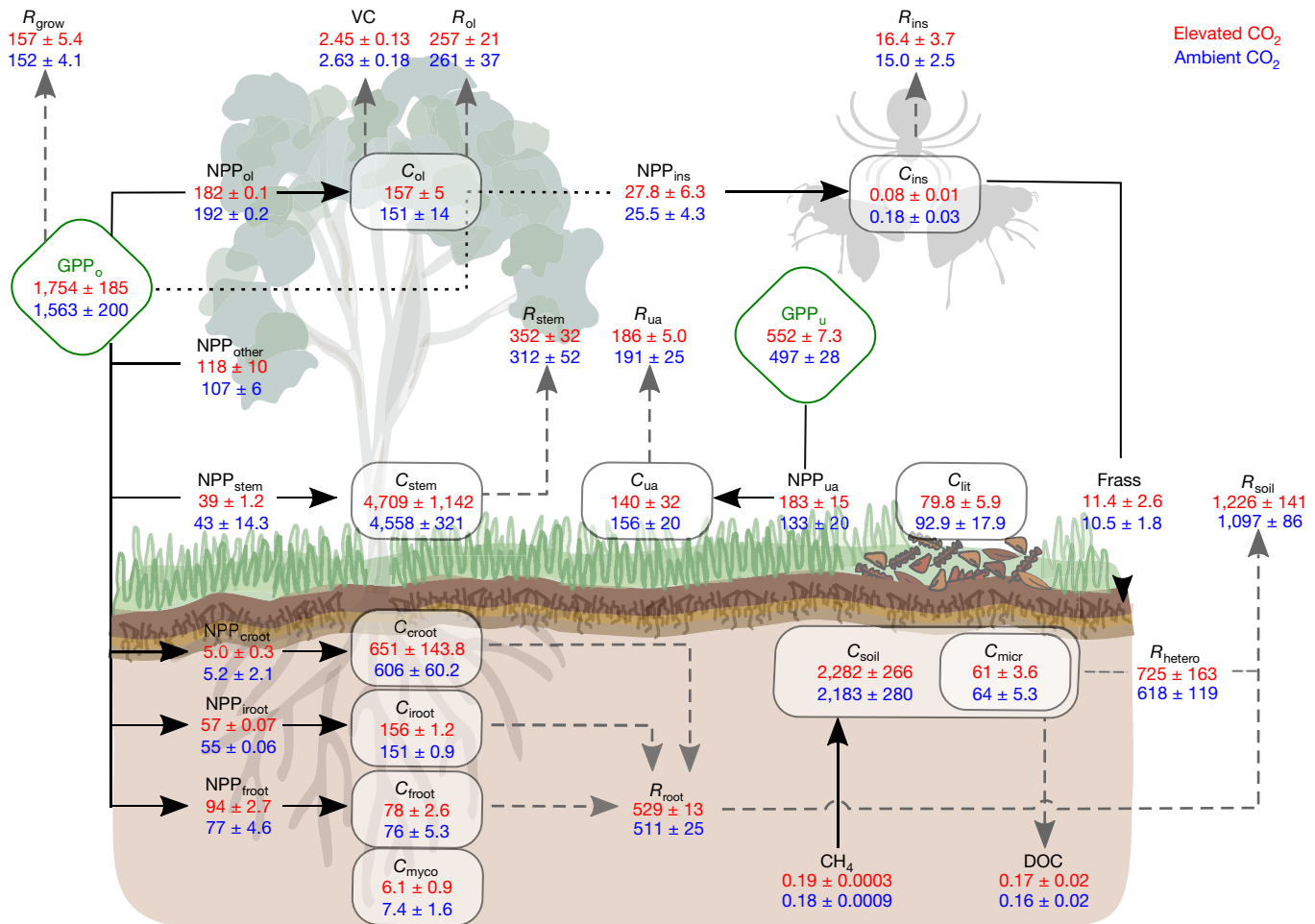


Fig. 1 | A comprehensive carbon budget under ambient and elevated CO₂ treatment in a mature forest ecosystem. Diamond-shaped boxes are gross primary production for overstorey (GPP_o) and understorey (GPP_u), respectively. Oval-shaped boxes are average carbon stocks over the experimental period (C_{pool}), including overstorey leaf (C_{ol}), stem (C_{stem}), coarse root (C_{croot}), fine root (C_{froot}), intermediate root (C_{iroot}), understorey aboveground (C_{ua}), leaf litter (C_{lit}), soil (C_{soil}), microbe (C_{micr}), aboveground insect (C_{ins}), and mycorrhizae (C_{myco}). Unboxed variables are carbon fluxes, including net primary production of overstorey leaf (NPP_{ol}), stem (NPP_{stem}), coarse root (NPP_{croot}), fine root (NPP_{froot}), intermediate root (NPP_{iroot}), and understorey aboveground (NPP_{ua}), overstorey leaf consumption by insects

(NPP_{ins}), respiration fluxes of overstorey leaf (R_{ol}), stem (R_{stem}), root (R_{root}), understorey aboveground (R_{ua}), growth (R_{grow}), insect (R_{ins}), heterotroph (R_{hetero}) and soil (R_{soil}), and volatile carbon emission (VC), frass production (Frass), dissolved organic carbon (DOC), and soil methane net uptake (CH_4). Lines with solid arrows are fluxes entering a pool; lines with dotted arrows are fluxes leaving a pool. The changes in each carbon pool over time (ΔC_{pool}) are reported in Extended Data Fig. 6. Blue values (bottom) are means \pm one standard deviation of the ambient CO₂ treatment ($n=3$), whereas red values (top) are means \pm one standard deviation of the elevated CO₂ treatment ($n=3$). All values are normalized by a linear mixed model with plot-specific pre-treatment LAI as a covariate to account for pre-existing differences.

is a crucial step towards quantifying the future carbon sequestration capacity of mature forests. To do so, we need to identify the fate of the extra carbon fixed under eCO₂ in mature forests, which are expected to be closer to a state of equilibrium between carbon uptake and turnover, compared to young aggrading stands.

The *Eucalyptus*FACE (EucFACE) experiment is a replicated, ecosystem-scale mature forest FACE experiment (Extended Data Figs. 1, 2). It is located in a warm-temperate evergreen forest that has remained undisturbed for the past 90 years, is dominated by the regionally widespread tree *Eucalyptus tereticornis* and has an understorey composed principally of native grasses and shrubs. The low-fertility soil has been shown to limit tree growth in an adjacent phosphorus-fertilization experiment¹⁷. Seven ecosystem-scale models were used to predict the eCO₂ response at EucFACE in advance of the experiment¹⁸, highlighting three alternative hypotheses for the expected ecosystem response based on plausible assumptions incorporated in different models¹⁹. These hypotheses were: (1) that enhanced photosynthesis under eCO₂ would lead to increased biomass accumulation; (2) that eCO₂-induced increase

in photosynthesis would be directly downregulated by limited nutrient availability; or (3) that eCO₂-induced increase in photosynthesis would lead to increased autotrophic respiration¹⁸. This range of predictions in a suite of well tested models indicated a prognostic knowledge gap as to how the carbon cycling of mature forests would respond to the expected rise in atmospheric CO₂ concentration¹¹, which is crucial to resolve in the face of future carbon-climate uncertainty²⁰.

So far, both canopy trees and understorey plants at EucFACE have shown increased rates of leaf photosynthesis but the canopy trees showed no statistically significant increase in aboveground biomass growth under eCO₂ ($P=0.43$, 95% CI=[−25%, +7%]; ref.⁷), reflecting a similar lack of response observed in other eCO₂ experiments on mature trees^{8–10}. Incorporating leaf-scale gas exchange measurements into a process-based tree stand model, it was estimated that the observed +19% stimulation of light-saturated overstorey leaf photosynthesis⁷ corresponded to a +11% stimulation of overstorey canopy gross primary production (GPP) in response to eCO₂ (ref.²¹). However, the probable fate of the extra carbon fixed under eCO₂ remained undetermined. Where did the extra carbongo?

To answer this question, we compiled measurements on all major carbon pools and fluxes collected over four years of experimental treatment (2013–2016), including individual and aggregated biomass and associated fluxes measured or inferred from plants, litter, soil, microbes and insects, and constructed an ecosystem carbon budget (Fig. 1) under both ambient ($a\text{CO}_2$) and $e\text{CO}_2$ conditions (+150 parts per million, ppm). We first confirmed the mass balance of the ecosystem carbon budget by checking agreement between independent estimates of GPP and soil respiration (R_{soil}) derived from separate data streams (Extended Data Fig. 3; see Methods). For the GPP of the $a\text{CO}_2$ plots, we confirmed that a process-based model estimate of overstorey and understorey GPP ($2,059 \pm 211 \text{ g C m}^{-2} \text{ yr}^{-1}$; mean \pm one standard deviation), driven by site-specific meteorology and treatment-specific physiological data, broadly agreed with the sum of data-driven estimates of net primary production (NPP) and autotrophic respiration ($2,068 \pm 61 \text{ g C m}^{-2} \text{ yr}^{-1}$). The carbon-use efficiency (NPP/GPP) of this mature forest was estimated to be 0.31 ± 0.03 , which is on the low end of global forest estimates, but is consistent with studies that have observed this ratio to decline with stand age²² (Extended Data Fig. 2). We further confirmed carbon mass balance for R_{soil} of the $a\text{CO}_2$ plots by comparing soil chamber-based estimates ($1,097 \pm 86 \text{ g C m}^{-2} \text{ yr}^{-1}$) with the sum of litterfall and independently estimated root respiration ($1,086 \pm 14 \text{ g C m}^{-2} \text{ yr}^{-1}$), assuming no change in soil carbon pool (see Methods). This agreement between independent estimates of components of the ecosystem carbon budget gives confidence that our measurements captured the pools and fluxes of carbon with low aggregate uncertainty and hence allow us to infer the fate of the extra carbon fixed under $e\text{CO}_2$.

To accommodate the inherent pre-treatment plot differences (see Methods), we normalized the CO_2 responses across plots by using a linear mixed model with plot-specific pre-treatment leaf area index (LAI) as a covariate^{23,24}. The non-normalized $e\text{CO}_2$ responses are provided in Extended Data Fig. 4, and generally confirm the findings but with larger uncertainty. Our normalized responses (Fig. 2, Extended Data Fig. 5) showed that $e\text{CO}_2$ induced an average of 12% increase ($+247 \pm 195 \text{ g C m}^{-2} \text{ yr}^{-1}$; difference of means \pm one standard deviation) in carbon uptake, including contributions of overstorey ($+192 \pm 193 \text{ g C m}^{-2} \text{ yr}^{-1}$) and understorey GPP ($+55 \pm 21 \text{ g C m}^{-2} \text{ yr}^{-1}$). The fate of this additional carbon entering the system under $e\text{CO}_2$ was primarily traced to an increase in R_{soil} ($+128.8 \pm 116.7 \text{ g C m}^{-2} \text{ yr}^{-1}$, or 52% of the carbon uptake surplus), followed by a smaller increase in tree stem respiration (R_{stem} ; $+40.0 \pm 43.6 \text{ g C m}^{-2} \text{ yr}^{-1}$, or 16% of the carbon uptake surplus). In comparison, the increase in total NPP ($+67.3 \pm 12.7 \text{ g C m}^{-2} \text{ yr}^{-1}$, or 28% of the carbon uptake surplus) corresponded to a smaller increase in storage of the total carbon pools at the ecosystem-level (ΔC_{pool} ; $+31.6 \pm 188.8 \text{ g C m}^{-2} \text{ yr}^{-1}$, or 12.8% of the carbon uptake surplus; Extended Data Fig. 6). There was thus little evidence of additional carbon accumulation under $e\text{CO}_2$ in this mature forest ecosystem. We then compared three alternative methods (see Methods) of estimating net ecosystem production (NEP) (Fig. 3). All three indicated that the ecosystem remained close to carbon-neutral under ambient CO_2 over the experimental period (mean \pm standard deviation for each method: $28 \pm 225 \text{ g C m}^{-2} \text{ yr}^{-1}$, $21 \pm 129 \text{ g C m}^{-2} \text{ yr}^{-1}$ and $-73 \pm 50 \text{ g C m}^{-2} \text{ yr}^{-1}$, respectively), and that $e\text{CO}_2$ of +150 ppm did not result in statistically significant increases in ecosystem carbon storage ($109 \pm 258 \text{ g C m}^{-2} \text{ yr}^{-1}$, $-19 \pm 171 \text{ g C m}^{-2} \text{ yr}^{-1}$ and $-42 \pm 262 \text{ g C m}^{-2} \text{ yr}^{-1}$, respectively). However, the variability reported here means that we cannot fully rule out the possibility of additional carbon storage under $e\text{CO}_2$, but we stress that our individual and aggregated responses consistently suggest a lack of CO_2 response in this mature forest (Figs. 2, 3 and Extended Data Fig. 5).

The relatively small but positive NPP response to $e\text{CO}_2$ was mainly driven by the understorey aboveground NPP response (NPP_{ua} ; $+50.3 \pm 17.9 \text{ g C m}^{-2} \text{ yr}^{-1}$), which was 75% of the net NPP response (Fig. 2). However, this NPP_{ua} response did not result in an equivalent $e\text{CO}_2$ effect on understorey aboveground biomass increment

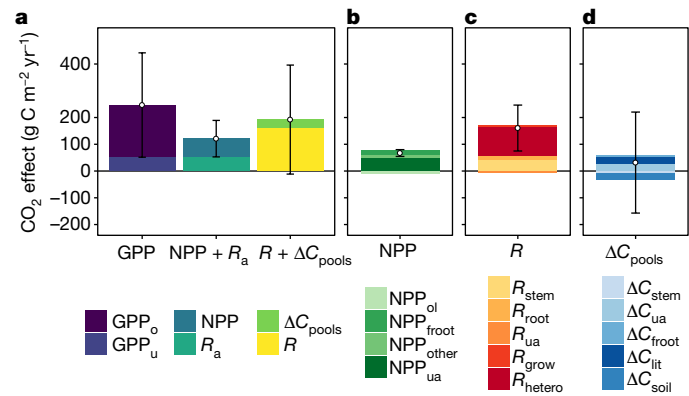


Fig. 2 | The fate of additional carbon fixed under $e\text{CO}_2$ in a mature forest ecosystem. **a**, GPP represents the total $e\text{CO}_2$ -induced increases in overstorey and understorey gross primary production (GPP_o and GPP_u , respectively); NPP + R_a represents the sum of net primary production and autotrophic respiration response; $R + \Delta C_{\text{pool}}$ represents the sum of ecosystem respiration and change in carbon storage response. **b**, The relative contributions of individual NPP fluxes to the aggregated NPP response to $e\text{CO}_2$, including NPP responses of overstorey leaf (NPP_{ol}), twigs, barks and seeds (NPP_{other}), fine root (NPP_{froot}), and understorey aboveground (NPP_{ua}). **c**, The relative contributions of individual respiratory fluxes to the aggregated R response to $e\text{CO}_2$, including respiration responses of stem (R_{stem}), root (R_{root}), understorey aboveground (R_{ua}), growth (R_{grow}), and soil heterotroph (R_{hetero}). **d**, The relative contributions of individual change in carbon storage to the aggregated ΔC_{pool} response to $e\text{CO}_2$, including changes in pool of stem (ΔC_{stem}), understorey aboveground (ΔC_{ua}), fine root (ΔC_{froot}), leaf litter (ΔC_{lit}), and soil (ΔC_{soil}). Variables with an absolute mean CO_2 effect of $<5 \text{ g C m}^{-2} \text{ yr}^{-1}$ are not reported in the bar chart. Individual CO_2 responses are reported in Extended Data Fig. 5. Each colour represents the CO_2 response of a flux variable, the point indicates the net sum of all variables for a column, and the error bar represents one standard deviation of the estimated column sum at the plot level (see Methods). The CO_2 effect is estimated using a linear mixed-model analysis with plot-specific pre-treatment LAI as a covariate to account for pre-existing differences (see Methods). The non-normalized response is provided in Extended Data Fig. 4, which agrees in general with the findings present in this figure, but with larger uncertainty.

($+27.2 \pm 29.7 \text{ g C m}^{-2} \text{ yr}^{-1}$), suggesting a possible higher understorey biomass turnover under $e\text{CO}_2$. Smaller fluxes, often neglected in other ecosystem carbon budgets, such as leaf consumption by insect herbivores (NPP_{ins} ; $25.5 \pm 4.3 \text{ g C m}^{-2} \text{ yr}^{-1}$ versus $27.8 \pm 6.3 \text{ g C m}^{-2} \text{ yr}^{-1}$, $a\text{CO}_2$ versus $e\text{CO}_2$ mean \pm standard deviation), insect frass production (Frass; $10.5 \pm 1.8 \text{ g C m}^{-2} \text{ yr}^{-1}$ versus $11.4 \pm 2.6 \text{ g C m}^{-2} \text{ yr}^{-1}$), vegetation volatile carbon emission (VC; $2.63 \pm 0.18 \text{ g C m}^{-2} \text{ yr}^{-1}$ versus $2.45 \pm 0.13 \text{ g C m}^{-2} \text{ yr}^{-1}$), net ecosystem methane uptake (CH_4 ; $0.18 \pm 0.0009 \text{ g C m}^{-2} \text{ yr}^{-1}$ versus $0.19 \pm 0.0003 \text{ g C m}^{-2} \text{ yr}^{-1}$), and leaching of dissolved organic carbon (DOC; $0.16 \pm 0.017 \text{ g C m}^{-2} \text{ yr}^{-1}$ versus $0.17 \pm 0.024 \text{ g C m}^{-2} \text{ yr}^{-1}$), contributed to the closure of the overall ecosystem carbon budget (Fig. 1; Extended Data Fig. 3), but were not quantitatively important in explaining pathways of the carbon uptake surplus under $e\text{CO}_2$ (Fig. 2, Extended Data Figs. 5, 6).

Here we provide replicated experimental evidence for the probable fate of carbon under $e\text{CO}_2$ in intact mature forest. We found that increased R_{soil} accounted for about half of the extra photosynthate produced by plants under $e\text{CO}_2$. It has been suggested that the increase in R_{soil} at EucFACE was probably a consequence of increased root and rhizosphere respiration^{25,26}, in contrast to other FACE sites where increased R_{soil} was attributed to enhanced soil organic matter decomposition (for example, DukeFACE²⁷). Here, the $e\text{CO}_2$ -induced increase in R_{soil} was not accompanied by substantial changes in root respiration ($18.6 \pm 20.1 \text{ g C m}^{-2} \text{ yr}^{-1}$) or in carbon pools associated with fine roots ($+7.0 \pm 12.5 \text{ g C m}^{-2} \text{ yr}^{-1}$), microbes ($+1.9 \pm 3.5 \text{ g C m}^{-2} \text{ yr}^{-1}$), mycorrhizae ($+0.4 \pm 0.5 \text{ g C m}^{-2} \text{ yr}^{-1}$), leaf litter ($+27.1 \pm 38.6 \text{ g C m}^{-2} \text{ yr}^{-1}$)

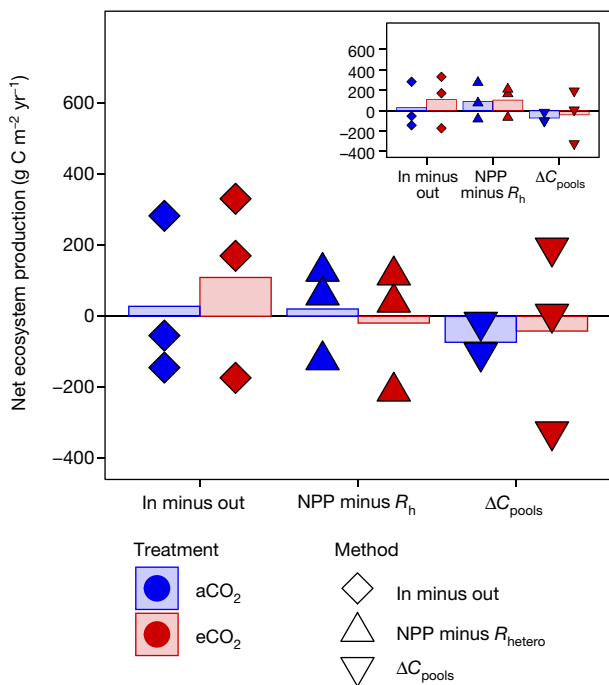


Fig. 3 | Estimates of NEP under ambient and elevated CO₂ treatment at EucFACE. Positive values indicate ecosystem net carbon uptake by the ecosystem. ‘In minus out’ calculates NEP based on the difference between total influxes and total outfluxes. ‘NPP minus R_{hetero} ’ calculates NEP based on the difference between net primary production (NPP) and heterotrophic respiration (R_{hetero}). ΔC_{pool} derives NEP based on incremental changes in all ecosystem carbon pools. Coloured bars indicate treatment means based on each method ($n = 3$), with blue representing ambient and red representing elevated CO₂ treatment. Individual dots are plot-level NEP, derived using different methods (see Methods). Values are normalized by a linear mixed model with plot-specific pre-treatment LAI as a covariate to account for pre-existing differences. The horizontal line indicates that NEP equals zero. The inset figure includes an inferred production allocation flux to mycorrhizal fungi (NPP_{myco}) based on data assimilation (Methods), which affected NEP estimates based on the ‘NPP minus R_{hetero} ’ method only.

or soil ($-23.8 \pm 159.6 \text{ g C m}^{-2} \text{ yr}^{-1}$), suggesting that the additional carbon fixed under eCO₂ may have led to an enhanced carbon transport belowground and a rapid belowground turnover of this flux. Assimilation of these data into a carbon balance model supports this inference (Extended Data Fig. 7; see Methods for details). An initial enhancement in nitrogen and phosphorus mineralization was observed²⁸, which suggested that the increased R_{soil} with eCO₂ could reflect soil organic matter priming with the potential to alleviate plant nutrient stress in this low-phosphorus soil^{28,29}. However, the enhanced soil mineralization rate and associated increase in nutrient availability did not persist over time²⁸, indicating that this increased belowground carbon allocation and the rapid turnover of this flux was not effective in increasing phosphorus availability to the plants³⁰.

The ecosystem carbon budget presented here provides an opportunity to confront the three alternative hypotheses of the response of this system to eCO₂ treatment that emerged from model predictions made in advance of the experiment¹⁸. Our data do not support any of the three hypotheses. The eCO₂-induced increase in photosynthesis was not strongly downregulated by low nutrient availability^{7,21}; nor did the eCO₂-induced additional carbon uptake lead to additional biomass accumulation, or enhanced aboveground respiration. These predictions reflect common mechanisms by which terrestrial vegetation models implement nutrient limitation of the eCO₂ response^{18,19,31,32}. In contrast, our results suggest a direct connection between plant photosynthesis and belowground activity (Extended Data Fig. 7), in which

increased belowground carbon allocation increased soil respiration at a rate that accounted for half of the extra carbon fixed under eCO₂ (Fig. 2). Predictions made in advance of the experiment did not capture this additional belowground carbon flux, despite their general agreement with data on turnover rates of major carbon pools (Extended Data Fig. 8). This increased soil respiration has been demonstrated by some models to be an important and often overlooked mechanism that reduces global soil carbon sequestration relative to estimates by many current models³³. As a consequence of including this rapid turnover of the increased belowground carbon allocation in terrestrial biosphere models, the time-lag in emitting some of the extra carbon via biomass accumulation and litterfall input into the soils may be reduced, thereby leading to faster cycling of carbon³⁴ and therefore possible different trajectories of carbon-climate predictions for the future.

A major form of land-based climate mitigation actions envisaged in the 2015 Paris Agreement is to enhance forest biomass carbon stocks globally through the protection of existing, largely mature, forests, and through afforestation of new areas. The mitigation potential of forests lies in the accumulated stock of ecosystem carbon, not in the short-term rate of forest photosynthesis. The probable fate of additional carbon determined in our study (Fig. 2) challenges the current thinking that non-aggrading mature forests will generally contribute to enhanced carbon sinks due to CO₂ fertilization³⁵, which further questions the allowable CO₂ emission targets sourced from existing carbon cycle models^{13,36}. Given that the effect of CO₂ fertilization may be one of diminishing returns over time¹⁴, the lack of eCO₂ effect on NEP (Fig. 3), if representative of nutrient-limited mature forest ecosystems generally, suggests an even weaker carbon sink in the future, especially in low-phosphorus systems such as EucFACE. Future research efforts should target a deeper understanding of the nutrient-carbon feedbacks that probably constrain the carbon sink potential of mature forests under eCO₂, and evaluate the implications of a potentially weaker terrestrial land carbon sink in the development of robust mitigation strategies in the face of climate change. More importantly, while the terrestrial carbon sink is integral to current strategies for climate change mitigation, our results call for more active reductions of anthropogenic emissions to meet the targets of the Paris Agreement.

Online content

Any methods, additional references, Nature Research reporting summaries, source data, extended data, supplementary information, acknowledgements, peer review information; details of author contributions and competing interests; and statements of data and code availability are available at <https://doi.org/10.1038/s41586-020-2128-9>.

1. Le Quéré, C. L. et al. Global carbon budget 2018. *Earth Syst. Sci. Data* **10**, 2141–2149 (2018).
2. Schimel, D., Stephens, B. B. & Fisher, J. B. Effect of increasing CO₂ on the terrestrial carbon cycle. *Proc. Natl Acad. Sci. USA* **112**, 436–441 (2015).
3. Walker, A. P. et al. Decadal biomass increment in early secondary successional woody ecosystems is increased by CO₂ enrichment. *Nat. Commun.* **10**, 454 (2019).
4. Norby, R. J. & Zak, D. R. Ecological lessons from Free-Air CO₂ Enrichment (FACE) experiments. *Annu. Rev. Ecol. Evol. Syst.* **42**, 181–203 (2011).
5. Leuzinger, S. & Härtenschwiler, S. Beyond global change: lessons from 25 years of CO₂ research. *Oecologia* **171**, 639–651 (2013).
6. Arora, V. K. et al. Carbon-concentration and carbon-climate feedbacks in CMIP5 Earth system models. *J. Clim.* **26**, 5289–5314 (2013).
7. Ellsworth, D. S. et al. Elevated CO₂ does not increase eucalypt forest productivity on a low-phosphorus soil. *Nat. Clim. Chang.* **7**, 279–282 (2017).
8. Körner, C. et al. Carbon flux and growth in mature deciduous forest trees exposed to elevated CO₂. *Science* **309**, 1360–1362 (2005).
9. Ryan, M. G. Three decades of research at Flakaliden advancing whole-tree physiology, forest ecosystem and global change research. *Tree Physiol.* **33**, 1123–1131 (2013).
10. Klein, T. et al. Growth and carbon relations of mature *Picea abies* trees under 5 years of free-air CO₂ enrichment. *J. Ecol.* **104**, 1720–1733 (2016).
11. Norby, R. J. et al. Model-data synthesis for the next generation of forest free-air CO₂ enrichment (FACE) experiments. *New Phytol.* **209**, 17–28 (2016).
12. Pugh, T. A. M. et al. Role of forest regrowth in global carbon sink dynamics. *Proc. Natl Acad. Sci. USA* **116**, 4382–4387 (2019).

13. Grassi, G. et al. The key role of forests in meeting climate targets requires science for credible mitigation. *Nat. Clim. Chang.* **7**, 220–226 (2017).
14. Peñuelas, J. et al. Shifting from a fertilization-dominated to a warming-dominated period. *Nat. Ecol. Evol.* **1**, 1438–1445 (2017).
15. Luo, Y. et al. Progressive nitrogen limitation of ecosystem response to rising atmospheric carbon dioxide. *Bioscience* **54**, 731–739 (2004).
16. DeLucia, E. H. et al. Net primary production of a forest ecosystem with experimental CO₂ enrichment. *Science* **284**, 1177–1179 (1999).
17. Crous, K., Ósväldsson, A. & Ellsworth, D. S. Is phosphorus limiting in a mature *Eucalyptus* woodland? Phosphorus fertilization stimulates stem growth. *Plant Soil* **391**, 293–305 (2015).
18. Medlyn, B. E. et al. Using models to guide field experiments: a priori predictions for the CO₂ response of a nutrient- and water-limited native eucalypt woodland. *Glob. Change Biol.* **22**, 2834–2851 (2016).
19. Medlyn, B. E. et al. Using ecosystem experiments to improve vegetation models. *Nat. Clim. Chang.* **5**, 528–534 (2015).
20. Friedlingstein, P. et al. Uncertainties in CMIP5 climate projections due to carbon cycle feedbacks. *J. Clim.* **27**, 511–526 (2014).
21. Yang, J. et al. Low sensitivity of gross primary production to elevated CO₂ in a mature eucalypt woodland. *Biogeosciences* **17**, 265–279 (2020).
22. DeLucia, E. H., Drake, J. E., Thomas, R. B. & Gonzalez-Meler, M. Forest carbon use efficiency: is respiration a constant fraction of gross primary production? *Glob. Change Biol.* **13**, 1157–1167 (2007).
23. Norby, R. J. Forest canopy productivity index. *Nature* **381**, 564 (1996).
24. Duursma, R. A. et al. Canopy leaf area of a mature evergreen *Eucalyptus* woodland does not respond to elevated atmospheric CO₂ but tracks water availability. *Glob. Change Biol.* **22**, 1666–1676 (2016).
25. Drake, J. E. et al. Short-term carbon cycling responses of a mature eucalypt woodland to gradual stepwise enrichment of atmospheric CO₂ concentration. *Glob. Change Biol.* **22**, 380–390 (2016).
26. Drake, J. E. et al. Three years of soil respiration in a mature eucalypt woodland exposed to atmospheric CO₂ enrichment. *Biogeochemistry* **139**, 85–101 (2018).
27. Drake, J. E. et al. Increases in the flux of carbon belowground stimulate nitrogen uptake and sustain the long-term enhancement of forest productivity under elevated CO₂. *Ecol. Lett.* **14**, 349–357 (2011).
28. Hasegawa, S., Macdonald, C. A. & Power, S. A. Elevated carbon dioxide increases soil nitrogen and phosphorus availability in a phosphorus-limited *Eucalyptus* woodland. *Glob. Change Biol.* **22**, 1628–1643 (2016).
29. Ochoa-Hueso, R. et al. Rhizosphere-driven increase in nitrogen and phosphorus availability under elevated atmospheric CO₂ in a mature *Eucalyptus* woodland. *Plant Soil* **416**, 283–295 (2017).
30. Crous, K. Y., Wujeska-Klause, A., Jiang, M., Medlyn, B. E. & Ellsworth, D. S. Nitrogen and phosphorus retranslocation of leaves and stemwood in a mature *Eucalyptus* forest exposed to 5 years of elevated CO₂. *Front. Plant Sci.* **10**, 664 (2019).
31. Zaehle, S. et al. Evaluation of 11 terrestrial carbon-nitrogen cycle models against observations from two temperature Free-Air CO₂ Enrichment studies. *New Phytol.* **202**, 803–822 (2014).
32. Fleischer, K. et al. Amazon forest response to CO₂ fertilization dependent on plant phosphorus acquisition. *Nat. Geosci.* **12**, 736–741 (2019).
33. Todd-Brown, K. E. O. et al. Changes in soil organic carbon storage predicted by earth system models during the 21st century. *Biogeosciences* **11**, 2341–2356 (2014).
34. Kuzyakov, Y., Horwath, W. R., Dorodnikov, M. & Blagodatskaya, E. Review and synthesis of the effects of elevated atmospheric CO₂ on soil processes: no changes in pools, but increased fluxes and accelerated cycles. *Soil Biol. Biochem.* **128**, 66–78 (2019).
35. Luyssaert, S. et al. Old-growth forests as global carbon sinks. *Nature* **455**, 213–215 (2008).
36. Jones, C. et al. 21st century compatible CO₂ emissions and airborne fraction simulated by CMIP5 Earth System models under 4 representative concentration pathways. *J. Clim.* **26**, 4398–4413 (2013).

Publisher's note Springer Nature remains neutral with regard to jurisdictional claims in published maps and institutional affiliations.

© The Author(s), under exclusive licence to Springer Nature Limited 2020

¹Hawkesbury Institute for the Environment, Western Sydney University, Penrith, New South Wales, Australia. ²Department of Sustainable Resources Management, College of Environmental Science and Forestry, State University of New York, Syracuse, NY, USA.

³Department of Ecology, Environment and Evolution, La Trobe University, Bundoora, Victoria, Australia. ⁴Arthur Rylah Institute for Environmental Research, Department of Environment, Land, Water and Planning, Heidelberg, Victoria, Australia. ⁵ARC Centre of Excellence for Climate Extremes, University of New South Wales, Sydney, New South Wales, Australia.

⁶Climate Change Research Centre, University of New South Wales, Sydney, New South Wales, Australia. ⁷Evolution and Ecology Research Centre, University of New South Wales, Sydney, New South Wales, Australia. ⁸Plant Biochemistry Laboratory, Department of Plant and Environmental Sciences, University of Copenhagen, Copenhagen, Denmark. ⁹VILLUM Research Center for Plant Plasticity, University of Copenhagen, Copenhagen, Denmark.

¹⁰Climate Science Centre, CSIRO Oceans and Atmosphere, Aspendale, Victoria, Australia. ¹¹Basque Centre for Climate Change, Leioa, Spain. ¹²Ikerbasque, Basque Foundation for Science, Bilbao, Spain. ¹³Department of Forest Ecology and Management, Swedish University of Agricultural Sciences (SLU), Umeå, Sweden. ¹⁴Estonian University of Life Sciences, Tartu, Estonia. ¹⁵Department of Geography, Indiana University, Bloomington, IN, USA. ¹⁶Forest Technology and Management Research Center, National Institute of Forest Science, Pocheon, South Korea. ¹⁷Department of Biology, IVAGRO, University of Cádiz, Campus de Excelencia Internacional Agroalimentario (CeiA3), Cádiz, Spain. ¹⁸School of Biological Sciences, Washington State University, Pullman, WA, USA. ¹⁹Division of Plant and Soil Sciences, West Virginia University, Morgantown, WV, USA. ²⁰Department of Forest Resources, University of Minnesota, St Paul, MN, USA. ²¹Terrestrial Ecology Section, Department of Biology, University of Copenhagen, Copenhagen, Denmark. ²²Laboratory of Plant Ecology, Faculty of Bioscience Engineering, Ghent University, Ghent, Belgium. ²³Global Centre for Land Based Innovation, Western Sydney University, Penrith, New South Wales, Australia.

²⁴Department of Physical Geography and Ecosystem Science, Lund University, Lund, Sweden. ²⁵Max Planck Institute for Biogeochemistry, Jena, Germany. [✉]e-mail: m.jiang@westernsydney.edu.au; b.medlyn@westernsydney.edu.au

Methods

EucFACE site description

The EucFACE facility (Extended Data Fig. 1) is located in a mature evergreen *Eucalyptus* forest on an alluvial spodosol in western Sydney, Australia (33° 36' S, 150° 44' E). The site has been a remnant patch of native Cumberland Plain woodland since the 1880s and has remained unmanaged for at least the past 90 years, with *Eucalyptus tereticornis* Sm. as the dominant tree species (98% of the overstorey basal area). *Eucalyptus* trees occur naturally across Australia, accounting for 78% of native forest area in Australia³⁷ and are planted widely around the globe³⁸. Infrastructure for six large circular plots (490 m² each) was established in 2010. Starting on 18 September 2012, three plots were subjected to free-air CO₂ enrichment treatment using a computer-controlled pre-dilution method. The CO₂ concentrations at EucFACE were ramped up over a six-month period, increasing by +30 ppm every five weeks in discrete steps (+30 ppm, 60 ppm, 90 ppm, 120 ppm and 150 ppm). The full elevated CO₂ treatment of +150 ppm started on 6 February 2013 during daylight hours on all days of the year. The site is characterized by a humid temperate–subtropical transitional climate with a mean annual temperature of 17.5 °C and a mean annual precipitation of 800 mm (Supplementary Fig. 1). The soil is a Holocene alluvial soil of low fertility with low phosphorus content³⁹. Soil texture is a loamy sand (>75% sand content) up to 50 cm in depth. From a depth of about 50 cm to about 300 cm, soils are sandy clay loam, with >30% silt and clay. Average bulk density is 1.39 g cm⁻³, 1.69 g cm⁻³ and 1.71 g cm⁻³ for depths of 0–10 cm, 10–20 cm and 20–30 cm, respectively (Supplementary Fig. 2). Permanent groundwater depth is about 11 m below the soil surface³⁹. Understorey vegetation is a diverse mixture of 86 species including forbs, graminoids and shrubs⁴⁰. The dominant understorey species is *Microlaena stipoides*, a C₃ perennial grass that accounted for around 70% of the herbaceous biomass and responded rapidly to rainfall variability⁴¹.

We estimated plot-specific carbon pools and fluxes at EucFACE over the years 2013–2016 (Supplementary Table 1). We defined pools as a carbon reservoir and annual increments as the annual changes in the size of each reservoir. We compartmentalized the ecosystem into 11 carbon pools, namely overstorey leaf (C_{ol}), stem (C_{stem}), fine root (C_{root}), coarse root (C_{croot}), intermediate root (C_{iroot}), understorey aboveground (C_{ua}), soil (C_{soil}), microbe (C_{micr}), mycorrhizae (C_{myco}), leaf litter (C_{lit}) and aboveground insect (C_{ins}) carbon pools, and reported pool size in units of grams of carbon per square metre. We defined fluxes as components of the carbon flow through the system, and report them in units of grams of carbon per square metre per year; all annual incremental changes (Δ) in carbon pools were reported in the same units. We converted estimates of biomass into carbon content using variable-specific carbon fractions (f) defined in Supplementary Table 2. Below, we describe how each pool and flux was estimated.

Pools

The soil carbon pool (C_{soil} ; Supplementary Fig. 2) was estimated based on quarterly sampled soil carbon content (oven-dried at 40 °C for 48 h) and plot-specific soil bulk density at three depths (0–10 cm, 10–20 cm and 20–30 cm). Of the 15 dates when samples were taken, soil carbon content below the top 10 cm of soil was measured on three dates. To obtain a more accurate estimate of annual incremental change in soil carbon pool, we therefore reported soil carbon pool for the top 10 cm only. There were no temporal and eCO₂ trends in soil carbon content at deeper depths.

The overstorey leaf carbon pool (C_{ol} ; Supplementary Fig. 3) was estimated based on continuous measures of leaf area index (LAI) and specific leaf area (SLA, in square metres of leaf area per gram of leaf dry matter), following $C_{ol} = LAI \times SLA \times f_{ol}$, where f_{ol} is a carbon fraction constant for overstorey leaves (Supplementary Table 2). Daily averages of plot-specific LAI were estimated based on the attenuation of diffuse radiation

in a homogeneous canopy²⁴. The number of observations varies between days, depending on the number of 30-min cloudy periods. SLA was estimated based on time-series measures of leaf mass per area, and was then linearly interpolated to plot-specific daily values over time.

The stem carbon pool (C_{stem} ; Supplementary Fig. 4) was estimated on the basis of tree-specific height and diameter at breast height (DBH) measurements, and an allometric scaling relationship derived for *E. tereticornis*⁷⁴². DBH changes were measured repeatedly at roughly monthly intervals, at height 1.3 m. Bark was periodically removed from under the dendrometer bands—this effect on DBH was considered by calculating biomass once per year using December data only. Stem biomass data were summed for each plot and averaged over the plot area to obtain ground-based estimates, and these were then converted into C_{stem} using treatment-specific carbon fraction (Supplementary Table 2).

The understorey aboveground carbon pool (C_{ua} ; Supplementary Fig. 5) was estimated at 1–3-month intervals between February 2015 and December 2016 using non-destructive measurements of plant height obtained from stereo-photography⁴³. In each of the four 2 m × 2 m understorey monitoring subplots within each plot, stereo photographs were collected using a Bumblebee XB3 stereo camera (Point Grey Research) mounted about 2.4 m above the ground surface and facing vertically downwards towards the centre of the subplot. Stereo images were taken at dusk under diffuse light conditions to avoid measurement errors related to shadows from trees and EucFACE infrastructure. On each sampling date, three sets of stereo photographs were taken in each subplot to produce a large number (that is, hundreds of thousands) of understorey plant height estimates from which mean plant height (H_{mean} , in metres) was calculated for each plot. Understorey aboveground biomass (B_{ua} , in kilograms per square metre) for each plot was predicted from H_{mean} using an empirical model developed for the grassy understorey vegetation at EucFACE ($B_{ua} = 1.72 \times H_{mean} - 0.05$)⁴³. The four subplot-level estimates were averaged to obtain a plot-level estimate of B_{ua} , and then converted to an estimate of C_{ua} using a carbon fraction constant (Supplementary Table 2).

The root carbon pool (C_{root}) consists of fine root (C_{root}), intermediate root (C_{iroot}), and coarse root (C_{croot}) pools, with C_{root} defined as roots with diameters of <2 mm, C_{iroot} defined as roots with diameters of 2–3 mm, and the remaining roots defined as C_{croot} (Supplementary Fig. 6). The C_{root} pool includes roots of both overstorey and understorey vegetation. Total root biomass (B_{root}) was estimated based on an allometric relationship with stand basal area (derived from DBH) derived for Australian forest species⁴⁴, as follows: $\ln(B_{root}) = 0.787 \times \ln(DBH) + 1.218$.

Standing intermediate root (2–3 mm in diameter) and fine root biomass (<2 mm in diameter) were sampled in four subplots per plot at two depths (0–10 cm and 10–30 cm) in the year 2017, whereas only fine root biomass at the same depths with the same number of subplots was repeatedly sampled over the period 2014–2016 (ref. ²⁹). We estimated a depth-specific relationship between fine root biomass (<2 mm in diameter) and total root biomass <3 mm in diameter based on samples collected in 2017, and calculated the intermediate root biomass for the period 2014–2016 based on its corresponding fine root biomass. Coarse root biomass was then estimated as the net difference between the total allometrically derived root biomass and that of roots with diameter <3 mm. The fine, intermediate and coarse root biomass were multiplied by the corresponding carbon fraction constants to obtain C_{root} , C_{iroot} and C_{croot} , respectively (Supplementary Table 2).

The microbial carbon pool (C_{micr}) was estimated based on fumigation extraction and 0.5 M K₂SO₄ extraction as in ref. ²⁵, using samples taken at 0–10-cm soil depth over the period 2012–2015. Total organic carbon was determined on a Shimadzu TOC analyser (TOC-L TNM-L; Shimadzu), which was then multiplied by soil bulk density over the same soil depth to obtain C_{micr} (Supplementary Fig. 7a).

The mycorrhizal carbon pool (C_{myco}) for the top 10 cm of soil was estimated via measurements of colonization of mycorrhizal in-growth bags, carbon isotopic partitioning, microbial phospholipid fatty acid

abundance and C_{micr} . Nine 45- μm nylon mesh bags ($4\text{ cm} \times 5\text{ cm}$) filled with sand, which excluded roots but allowed access to fungi⁴⁵, were buried in November 2014 in each experimental plot and three bags were subsequently collected every four months for one year. Phospholipid-derived fatty acids (PLFA), a proxy for total microbial biomass abundance, were quantified in sand bags and native field soil following the protocol in ref.⁴⁶. $\delta^{13}\text{C}$ values of ground subsamples of this sand, native soil carbon and aboveground plant tissue (leaves of eucalypts in April 2014) were used to estimate the fraction of the accumulated carbon in sand bags that was derived from plant carbon using isotopic mass balance. Because roots were excluded, plant-derived carbon in bags can be attributed to mycorrhizae. This plant-derived unitless fraction was then multiplied by the total concentration of PLFA in sand bags to obtain the amount of the total PLFA contributed by mycorrhizae (micrograms of PLFA per gram of sand). To scale this to native soil PLFA concentrations we then calculated the ratio between mycorrhizal PLFA in sand bags to total PLFA in soil (representing the total microbial pool). Subsequently, to estimate C_{myco} , this ratio was multiplied by the C_{micr} in each plot (Supplementary Fig. 7b).

The leaf litter carbon pool (C_{litter}) was estimated based on the leaf litter decomposition rate and leaf litterfall data collected by litter baskets (Supplementary Fig. 8)²⁴. Leaf litter decomposition rates were estimated over 24 months using litter bags. Briefly, 2 g of air-dried *Eucalyptus* litter was added to $10\text{ cm} \times 15\text{ cm}$ litter bags with a 2-mm mesh size. Twelve litter bags were randomly allocated to 4 subplots within each treatment plot, and two litter bags were collected at 3, 6, 9, 12, 18 and 24 months to calculate mass loss over time (mass loss was averaged across the two replicates from each subplot). A leaf litter exponential decay function was estimated for each plot, based on data collected over this 24-month period. Leaf litterfall was estimated from monthly collections of material from circular fine-mesh traps (trap size 0.2 m^2) at eight random locations for each plot. We then applied the exponential decay function with litterfall biomass to obtain C_{litter} , assuming a carbon fraction constant (Supplementary Table 2).

The insect carbon pool (C_{ins}) was estimated based on two different sampling techniques, with aerial insects partially estimated based on monthly dead insect data collected from circular fine-mesh traps of size 0.2 m^2 at eight random locations for each plot⁴⁷, and understory insects estimated based on vacuum suction sampling from two locations for each plot⁴⁸. The insect biomass estimated based on these two sampling techniques may be a conservative estimate (the frass produced would suggest the presence of a larger insect biomass⁴⁹); nevertheless, they provided a direct estimate based on data collected *in situ*. The vacuum suction method collected invertebrates from understorey vegetation in two $1\text{ m} \times 1\text{ m}$ subplots using a petrol-powered 'G-Vac' vacuum device run on full throttle for 20 s, for a total of five sampling campaigns. Trapping locations were randomly chosen and fixed between sampling campaigns. All invertebrates were sorted from debris, dried to constant weight at $60\text{ }^\circ\text{C}$ and weighed on a microbalance with a precision of $1\text{ }\mu\text{g}$. We assumed that vacuum samples as well as fine-mesh trap samples represent point estimates of invertebrate abundance. The total biomass of sampled invertebrates was then summed across sampling methods within each plot. A constant carbon fraction based on ref.⁵⁰ (Supplementary Table 2) was used to convert biomass into the C_{ins} pool (Supplementary Fig. 9).

Ecosystem carbon uptake fluxes

The overstorey gross primary production (GPP_o) for each plot was provided by a stand-level model simulation (MAESPA), forced by hourly meteorological data, daily plot-specific LAI and leaf-scale treatment-specific photosynthetic parameters measured at the site (Supplementary Fig. 10a)^{7,21}. In short, MAESPA was used as a tool to scale up the leaf-level gas exchange measurements to the whole canopy. In MAESPA, each plot consists of individual tree crowns that are located and parameterized with measured coordinates, crown size and LAI. Each crown

is divided into six layers, with leaf area uniformly distributed in each layer. Within each layer, the model simulates twelve grid points. The incident radiation on the sunlit and shaded leaf area at each grid point is calculated taking into account shading from the upper crown and surrounding trees, the solar angle (zenith and azimuth) and the light source (diffuse or direct). Incident radiation is then used to calculate gas exchange using a Farquhar⁵¹ formulation for photosynthesis and a Medlyn formulation⁵² for stomatal conductance. The model was parameterized with treatment-specific leaf gas exchange measurements made *in situ*^{7,53}. Leaf respiration and its temperature dependence were also quantified using data collected on site, then scaled up to the canopy using MAESPA. The performance of the model was evaluated by comparing the simulated transpiration flux to sap-flow data⁵⁴.

Similarly, the understorey GPP (GPP_u) (Supplementary Fig. 10b) was simulated using MAESPA with photosynthetic parameters taken for the dominant grass *Microlaena stipoides*⁴¹. The parameterization of understorey vegetation is different from that of the canopy. In each plot, the understorey was assumed to form a single crown covering the whole plot (that is, a circle with radius 12.5 m) at a height of 1.5 m. The LAI of the understorey was estimated using phenology camera digital photographs taken at four permanent understorey vegetation monitoring subplots in each plot⁴³. The average green pixel content was calculated from three photographs in each subplot, and assumed to be the same as the fraction of absorbed photosynthetically active radiation. We then assumed a light extinction coefficient of 0.5 in Beers' Law and calculated understorey LAI. Before 2014 there were three campaigns per year whereas from 2014 the cameras were automated, and we used the fortnightly averages. Leaf gas exchange parameters were obtained from ref.⁴¹ and covered four to six campaigns per year from 2013 to 2016. We estimated a one-time g_1 parameter⁵² for all plots and time, and assumed constant carboxylation rate and electron transport rate values at $25\text{ }^\circ\text{C}$ across plots. Basal leaf respiration rate and the temperature dependence of photosynthesis and respiration were assumed to be the same as those for the canopy. The understorey simulation was conducted separately from the canopy, with canopy LAI from ref.²⁴ included to account for the shading from the canopy, branches and stems on the understorey.

For the methane net flux (CH_4), air samples were collected following the closed-chamber method: the non-flow-through non-steady-state (NFT-NSS) method. Seven replicated chambers were available for each plot. Headspace samples were collected monthly, over a period of one hour, and analysed by gas chromatography. Fluxes were estimated by a mixture of linear and quadratic regressions (depending on goodness of fit), assuming a constant air pressure of one atmosphere and correcting the air temperature inside the chambers for each air sample⁵⁵. The CH_4 fluxes are net fluxes, which represent the sum of: (1) CH_4 efflux (emissions from the soil into the atmosphere); and (2) CH_4 influx (uptake from the atmosphere into soil). Here, the annual net CH_4 flux was an ecosystem influx and was presented as positive values (Supplementary Fig. 11a).

Production fluxes

Plant net primary production (NPP) is the sum of overstorey leaf (NPP_{ol}), stem (NPP_{stem}), fine root (NPP_{froot}), intermediate root (NPP_{iroot}), coarse root (NPP_{croot}), other (including twigs, barks, and seeds; NPP_{other}), understorey aboveground (NPP_{ua}), and consumption of overstorey leaf by insect herbivores (NPP_{ins}). NPP_{ol} and NPP_{other} were estimated based on monthly litter data collected from circular fine-mesh traps of 0.2 m^2 at eight random locations for each plot (Supplementary Fig. 12). Litter was sorted into leaf, twigs, bark and seeds, dried to constant mass at $40\text{ }^\circ\text{C}$ and weighed. A subsample was reweighed when dried to constant mass at $70\text{ }^\circ\text{C}$ and a small moisture correction⁷ was applied to the leaf component of the whole dataset. NPP_{ol} was computed as the sum of annual leaf litter, which excluded leaf consumption by insects. For twigs, we assumed strictly annual turnover across the years. NPP_{stem} (Supplementary Fig. 13) and NPP_{croot} (Supplementary Fig. 14) were

Article

estimated based on the annual incremental change of stem biomass and coarse root biomass, respectively. NPP_{root} was estimated based on samples collected from in-growth cores at four different locations per plot (Supplementary Fig. 14). NPP_{root} was estimated based on a global mean coarse root turnover rate (0.3605 per year) for evergreen broad-leaved forests⁵⁶, and the C_{root} pool in our dataset (Supplementary Fig. 14).

NPP_{ua} was estimated based on biomass clippings taken between 2015 and 2017, assuming one understorey turnover per harvest interval (Supplementary Fig. 15). We used a clip-strip method of biomass harvest as was applied previously at the BioCON experiment⁵⁷. Specifically, four narrow strips, each with a size of 1 m × 0.1 m, were situated in each of the experimental plots at least 2 m away from the vertical pipes for FACE, while avoiding the understory shrubs. The understory herbaceous species were clipped approximately 1 cm above soil level. The total mass per harvest represents the total production. Biomass samples were oven dried for two days at 60 °C, and converted into carbon mass by applying a constant fraction (Supplementary Table 2).

NPP lost to overstorey leaf consumption by insect herbivores (NPP_{ins}) was estimated based on insect frass data (Frass) collected from the circular fine-mesh traps, and a relationship between frass mass and insect-consumed leaf mass derived based on multiple *Eucalyptus* tree species at different CO₂ concentrations (Supplementary Fig. 16a)^{58,59}. Frass was estimated based on annual collection of frass biomass collected from the circular fine-mesh litter traps with their associated carbon content (Supplementary Table 2 and Supplementary Fig. 16c).

Outfluxes

Leaching lost as dissolved organic carbon (DOC) from soils was estimated based on concentrations of DOC in soil solutions, provided by water suction lysimeter measurements²⁸. Lysimeters were installed to two depths (0–15 cm and 35–75 cm, which is immediately above the impermeable layer). Here we assumed that DOC reaching deeper depth is lost from the system at a rate of 20 ml m⁻² d⁻¹, which is an estimate of the daily drainage rate at the site (Supplementary Fig. 11b).

Plant autotrophic respiration (R_a) consists of overstorey leaf (R_o), stem (R_{stem}), root (R_{root}), understorey aboveground (R_{ua}) (Supplementary Fig. 17), and growth respiration (R_{grow}) (Supplementary Fig. 18). R_o and R_{ua} were based on MAESPA simulation (Supplementary Fig. 17a, c), as described in the respective GPP sections. R_{grow} was estimated by taking a constant fraction of 30% of total NPP as measured directly on *E. tereticornis* trees⁶⁰.

R_{stem} was estimated from measurements of stem CO₂ efflux performed in three dominant trees per plot (Supplementary Fig. 17b). Collars were horizontally attached to the stem at an approximate height of 0.75 m, and R_{stem} (in units of nmol CO₂ per square metre per second) was measured with a portable infrared gas analyser coupled to a soil respiration chamber adapted for this purpose⁶¹. Measurement campaigns were performed every one or two months from December 2017 to October 2018, and the relationship between R_{stem} and air temperature (T_{air}) was used to extrapolate R_{stem} across the surveyed period, following R_{stem} = 0.1866 × 2.84 T_{air}¹⁰ (r² = 0.42, P < 0.0001). R_{stem} was then scaled up to the stand level taking into account the ratio of stem axial surface per unit of soil surface measured per plot. Stem surface area was inferred from the measured tree diameter using a dendrometer, and a relationship between diameter and stem surface area estimated from the Terrestrial Laser Scanning (TLS) data. Stem surface area and diameter in the TLS data were estimated through quantitative structure models presented in refs.^{62,63}. TLS data were acquired with a RIEGL VC-400 terrestrial laser scanner (RIEGL Laser Measurement Systems). Stem surface area was derived from the TLS data following a two-step approach: (1) manually extracting single trees from the registered TLS point cloud; and then (2) deriving parameters for an extracted single tree. Once a tree was extracted from the point cloud, the next step was to strip off the leaves, and segment the point cloud into stem and branches. Finally, the surface of the segments was reconstructed with

geometric primitives (cylinders). The method used a cover set approach, where the point cloud was partitioned into small subsets, which correspond to small connected patches in the tree surface.

R_{root} was partitioned into fine root (R_{froot}), intermediate root (R_{iroot}), and coarse root (R_{croot}) respiration (Supplementary Fig. 17d). Mass-based rates of fine root and intermediate root respiration (in nanomoles of CO₂ per gram of root dry matter per second) were measured for detached roots sampled by soil cores at 10 cm soil depth at four subplots per plot with a portable infrared gas analyser coupled to a small root chamber. Measurement campaigns were performed every one or two months from November 2018 to July 2019. The relationship between root respiration and soil temperature (T_{soil}) at 10 cm soil depth was used to extrapolate the corresponding root respiration rates across the surveyed period, following the equations: R_{froot} = 1.138 × 1.614^{0.0479 T_{soil}} (correlation r² = 0.36, P < 0.0001, root mean square error RMSE = 1.054), and R_{iroot} = 0.9764 × 1.586^{0.0641 T_{soil}} (r² = 0.52, P < 0.0001, RMSE = 0.597). The mass-based rate of coarse root respiration was assumed to be the same as the mass-based rate of stem respiration. R_{froot}, R_{iroot} and R_{croot} were then scaled up to the stand level to obtain R_{root} with fine root, intermediate root and coarse root biomass, respectively. Carbon efflux due to insect respiration (R_{ins}) was estimated as the net difference between NPP_{ins} and Frass, assuming no net change in insect biomass (Supplementary Fig. 16b).

To determine soil respiration (R_{soil}), the rate of soil CO₂ efflux was measured at eight locations within each plot, where a permanent polyvinyl carbonate collar inserted into the soil was co-located with soil time domain reflectometry probes for continuous measurements of soil temperature (5 cm depth) and volumetric water content (0–21 cm depth; CS650-L; Campbell Scientific). R_{soil} was measured manually at all collar locations every 2–3 weeks, in addition to 30-min measurements using automated chambers (Li-8100-103; Licor) at one location within each plot, resulting in >300,000 observations over the study period²⁶. These data were used to parameterize a semi-mechanistic model of R_{soil}, in which R_{soil} was predicted based on measurements of soil properties, soil physics, and measured soil temperature and volumetric water content⁶⁴. This model successfully recreated the observed fluxes (r² between the predicted and observed survey R_{soil} values was 0.65)²⁶. Annual sums of R_{soil} were derived by summing the averaged daily fluxes over eight locations within each plot, where daily fluxes at each location were predicted based on the semi-mechanistic model and daily soil temperature and volumetric water content data taken adjacent to each measurement collar. Soil heterotrophic respiration (R_{hetero}) was taken as the net difference between R_{soil} and R_{root} (Supplementary Fig. 19). Total ecosystem respiration R was calculated as the sum of R_a, R_{hetero}, R_{ins} and VC.

The volatile carbon (VC; Supplementary Fig. 20) flux as isoprene (C₅H₈) and monoterpenes was estimated using the Model of Emissions of Gases and Aerosols from Nature (MEGAN)⁶⁵. Isoprene represents over half of all volatile organic carbon species emitted by vegetation globally, and is the dominant source of VC emission at our site. A MEGAN box-model was built from the version used in ref.⁶⁶, centred on the EucFACE facility to calculate hourly emissions of isoprene across the period 2013–2016 for all six plots: VC = EF × LAI × γ, where EF is the compound-specific landscape emission factor and γ is the emission activity factor, accounting for changes in the emission response caused by light, temperature, leaf age and soil moisture. The MEGAN simulations were driven by daily input data of LAI, soil moisture and hourly input data of photosynthetic active radiation, temperature, atmospheric pressure, wind speed and relative humidity.

The isoprene EF values for the ambient and elevated CO₂ plots were derived from in-line photosynthetic gas-exchange measurements coupled with simultaneous volatile isoprenoid sampling. The isoprene was collected onto sterile stainless steel thermal desorption tubes at the same time as gas exchange was measured, and these were capped and later thermally desorbed for off-line volatile analysis in the laboratory using a Shimadzu 2010 Plus GC-MS system connected to a Shimadzu TD20 automated cartridge desorber. The sampling and gas chromatograph/mass spectrometer (GC-MS) analysis methodology is described

in detail in ref.⁶⁷. The chromatographic peaks were identified by comparing them to an isoprene standard and reference mass spectra in the NIST Mass Spectral Library (<https://www.nist.gov/srd>). Monoterpene emissions were sampled during February 2018 using a push–pull head-space technique⁶⁸ from enclosed branches containing approximately 10 leaves and trapped on adsorbent cartridges (150 mg Tenax TA and 200 mg Carbograph 1TD, Markets International) at an outflow rate of 200 ml min⁻¹ for 15 min. Before each measurement, the sampling system was equilibrated for 15 min at an inflow rate of 1,000 ml min⁻¹. Monoterpenes were analysed by GC-MS (R7890A Series GC coupled with a 5975C inert MSD/DS Performance Turbo EI System, Agilent Technologies), as described by ref.⁶⁹. The chromatograms obtained were deconvoluted, analysed and data retrieved using the software PARADISE⁷⁰ version 3.88. Identification of compounds was performed using analytical standards and according to their mass spectra in the NIST11 library. Pure analytical standards were used for quantification. The MEGAN model produced isoprene and monoterpenes were converted to carbon content using their respective molecular mass ratios.

Net ecosystem production

NEP was estimated based on three different methods that estimated NEP in relatively independent ways (Fig. 3), similar to ref.⁷¹. The first method considered NEP as the difference between total ecosystem influx and total ecosystem outflux (In minus Out), which relied on both process-based modelling and empirical upscaling of respiratory fluxes collected from the field. The second method considered NEP as NPP minus R_{hetero} , with NPP relying mostly on litter-based production estimates, and R_{hetero} relying on R_{soil} and R_{root} estimates. The third method considers NEP as the sum of changes in carbon pools over time in the ecosystem (that is, ΔC_{pool}), which was mostly determined by biomass estimates. Equations for each method (In minus Out, NPP minus R_{hetero} and ΔC_{pool} , respectively) are provided below:

$$\text{NEP} = \text{GPP}_0 + \text{GPP}_u + \text{CH}_4 - R_{\text{ol}} - R_{\text{stem}} - R_{\text{soil}} - R_{\text{ua}} - R_{\text{ins}} - \text{DOC} - \text{VC} \\ - R_{\text{grow}}$$

$$\text{NEP} = \text{NPP}_{\text{ol}} + \text{NPP}_{\text{stem}} + \text{NPP}_{\text{froot}} + \text{NPP}_{\text{iroot}} + \text{NPP}_{\text{croot}} + \text{NPP}_{\text{other}} + \text{NPP}_{\text{ua}} \\ + \text{NPP}_{\text{ins}} - R_{\text{hetero}}$$

$$\text{NEP} = \Delta C_{\text{soil}} + \Delta C_{\text{ol}} + \Delta C_{\text{stem}} + \Delta C_{\text{croot}} + \Delta C_{\text{froot}} + \Delta C_{\text{iroot}} + \Delta C_{\text{ua}} + \Delta C_{\text{lit}} \\ + \Delta C_{\text{ins}} + \Delta C_{\text{micr}} + \Delta C_{\text{myco}}$$

Carbon budget evaluation

We evaluated the mass balance of our estimated ecosystem carbon budget in two ways. First, we compared model-simulated GPP with the aggregated sum of NPP and R_a (Extended Data Fig. 3a, b). GPP was simulated by a stand-level ecophysiological model, driven by hourly meteorological data and parameterized with site-specific ecological data²¹. This GPP should equal to the aggregation of NPP ($\text{NPP}_{\text{ol}} + \text{NPP}_{\text{stem}} + \text{NPP}_{\text{froot}} + \text{NPP}_{\text{iroot}} + \text{NPP}_{\text{croot}} + \text{NPP}_{\text{other}} + \text{NPP}_{\text{ua}} + \text{NPP}_{\text{ins}}$) and R_a fluxes ($R_{\text{ol}} + R_{\text{stem}} + R_{\text{root}} + R_{\text{ua}} + R_{\text{grow}}$), which were mostly extrapolated based on field data. Second, R_{soil} estimated from soil collar flux measurements²⁵ was evaluated against the sum of litterfall and R_{root} (Extended Data Fig. 3c, d), assuming minimal changes in soil carbon stock (as change over this short period of time is beyond the detection limit in a complex and slow-growing mature forest ecosystem like EucFACE). Here, litterfall was the sum of $\text{NPP}_{\text{ol}} + \text{NPP}_{\text{froot}} + \text{NPP}_{\text{iroot}} + \text{NPP}_{\text{other}} + \text{NPP}_{\text{ua}} + \text{Frass}$ and R_{root} was extrapolated on the basis of root biomass and temperature functions.

Statistical analyses

We performed a linear mixed-model analysis using the ‘lmer’ function within the ‘lme4’ package⁷² in the software package *R* (ref.⁷³) to

determine the CO₂ treatment effect on all reported variables. All fluxes were reported at an annual rate. In our model, date and CO₂ treatment were considered as fixed factors, plot as a random factor, and plot-specific pre-treatment LAI (that is, 4-month average LAI before full CO₂ treatment was switched on) as a covariate to account for pre-treatment differences among treatment plots. Normalizing all response variables with a covariate that integrates light, water and nutrient constraints helps to isolate the CO₂ effect²³, as has been done previously at the site²⁴ and elsewhere^{8,23}. Uncertainties for the predicted fluxes and pools are reported as the standard deviation of the plot-specific totals ($n = 3$). Standard deviations for the aggregated fluxes (for example, NPP) were calculated by summing the individual component fluxes that constitutes the aggregated flux for each plot and computing the standard deviations across plots ($n = 3$). Finally, standard deviations for the CO₂ effect size (SD_{eff}) of the individual and aggregated fluxes and pools (for example, NPP) were calculated by pooling the standard deviations of the ambient (SD_{amb}) and elevated CO₂ treatment (SD_{ele}), as follows:

$$\text{SD}_{\text{eff}} = \sqrt{\frac{\text{SD}_{\text{amb}}^2 + \text{SD}_{\text{ele}}^2}{2}}$$

We note that the reported standard deviations can be used to construct confidence intervals for the CO₂ effect size as (effect size $\pm t_{95}\text{SD}_{\text{eff}} n^{-1/2}$), where t_{95} is the critical value of the *t* distribution at 95%, and $n = 3$ is the sample size.

Uncertainty analysis

We applied a Markov Chain Monte Carlo (MCMC) data assimilation algorithm to a simplified carbon cycle framework to infer the uncertainties around the fate of carbon in our carbon budget. We simplified our carbon budget into eight pools (Extended Data Fig. 7), namely, leaf (C'_{leaf} , which includes overstorey and understorey), wood (C'_{wood} , which includes stem and coarse root), root (C'_{root} , which includes fine root and intermediate root), aboveground litter (C'_{aglit}), below-ground litter (C'_{bglit}), mycorrhizae (C'_{myco}), microbe (C'_{micr}), and soil (C'_{soil}). Here, C'_{aglit} and C'_{bglit} were assumed to be unknown and inferred from the analysis. The prime symbol is used to differentiate these simplified carbon budget variables from those presented in Fig. 1. NPP was calculated as the difference of GPP and autotrophic respiration R_a . NPP was then allocated into the four plant carbon pools (C'_{leaf} , C'_{wood} , C'_{root} , and C'_{myco}), with the respective fitted allocation coefficients (a_{leaf} , a_{wood} , a_{root} and a_{myco}) being inferred. It has been shown that plant carbon allocation to mycorrhizal fungi may be an important flux in forest carbon budget calculation⁷⁴. Turnover rates of C'_{leaf} , C'_{root} , C'_{myco} , C'_{aglit} , C'_{bglit} , C'_{micr} and C'_{soil} were represented by the corresponding turnover coefficients (τ_{leaf} , τ_{wood} , τ_{root} , τ_{myco} , τ_{aglit} , τ_{bglit} , τ_{micr} , τ_{soil}), all of which were assumed to be unknown except for τ_{wood} (estimated based on litter basket data of twigs, barks and seeds) and τ_{aglit} (estimated from the leaf litter decomposition data). For carbon leaving via C'_{aglit} , C'_{bglit} and C'_{micr} , we inferred the corresponding fractional coefficient that determines the fraction of carbon entering into the next pool (f'_{aglit} , f'_{bglit} and f'_{micr}), and assumed that the remainder was respired as part of R_{hetero} . The turnover of soil carbon (that is, τ_{soil}) also contributed to R_{hetero} . In total, we fitted two pools, four allocation coefficients, six turnover rates, and three fractional coefficients using the MCMC algorithm.

We used plot-level estimates of GPP, R_a , R_{hetero} , carbon pools and changes in pools to constrain the MCMC fitting. We assumed uniform parameter distributions and a burn-in coefficient of 10%. Chain lengths were set at 200,000 for the ambient CO₂ plots and 500,000 for the elevated plots. The longer chain length for the elevated plots was because of the smaller proposal step size for these plots to meet an acceptance rate of around 20%. We reported the means and standard deviation of the estimated parameters at the treatment level in Extended Data Fig. 7.

Data availability

Data included in this paper are available via Figshare (<https://doi.org/10.6084/m9.figshare.11634315.v1>).

Code availability

Codes for processing the data are available via GitHub (https://github.com/mingkaijiang/EucFACE_carbon_budget_paper.git).

37. Australia's Agriculture, Fisheries And Forestry At A Glance 2012 <https://www.agriculture.gov.au/about/publications/glance2012> (Department of Agriculture, Fisheries and Forestry, 2012).
38. Global Forest Resources Assessment 2000 FAO Forestry Paper 140 (Food and Agricultural Organization of the United Nations, 2001).
39. Gimeno, T. E., McVicar, T. R., O'Grady, A. P., Tissue, D. T. & Ellsworth, D. S. Elevated CO₂ did not affect the hydrological balance of a mature native *Eucalyptus* woodland. *Glob. Change Biol.* **24**, 3010–3024 (2018).
40. Hasegawa, S. et al. Elevated CO₂ concentrations reduce C₄ cover and decrease diversity of understorey plant community in a *Eucalyptus* woodland. *J. Ecol.* **106**, 1483–1494 (2018).
41. Pathare, V. S. et al. Water availability affects seasonal CO₂-induced photosynthetic enhancement in herbaceous species in a periodically dry woodland. *Glob. Change Biol.* **23**, 5164–5178 (2017).
42. Paul, K. I. et al. Development and testing of allometric equations for estimating above-ground biomass of mixed-species environmental plantings. *For. Ecol. Manage.* **310**, 483–494 (2013).
43. Collins, L. et al. Understorey productivity in temperate grassy woodland responds to soil water availability but not to elevated CO₂. *Glob. Change Biol.* **24**, 2366–2376 (2018).
44. Snowdon, P. et al. National Carbon Accounting System Technical Report no. 17 (Australian Greenhouse Office, 2000).
45. Wallander, H. et al. Evaluation of methods to estimate production, biomass and turnover of ectomycorrhizal mycelium in forests soils. *Soil Biol. Biochem.* **57**, 1034–1047 (2013).
46. Buyer, J. S. & Sasser, M. High throughput phospholipid fatty acid analysis of soils. *Appl. Soil Ecol.* **61**, 127–130 (2012).
47. Gherlenda, A. N., Esveld, J. L., Hall, A. A. G., Duursma, R. A. & Riegler, M. Boom and bust: rapid feedback responses between insect outbreak dynamics and canopy leaf area impacted by rainfall and CO₂. *Glob. Change Biol.* **22**, 3632–3641 (2016).
48. Facey, S. L. et al. Atmospheric change causes declines in woodland arthropods and impacts specific trophic groups. *Agric. For. Entomol.* **19**, 101–112 (2017).
49. Murray, T. J., Tissue, D. T., Ellsworth, D. S. & Riegler, M. Interactive effects of pre-industrial, current and future CO₂ and temperature on an insect herbivore of *Eucalyptus*. *Oecologia* **171**, 1025–1035 (2013).
50. Trakimas, G. et al. Ecological stoichiometry: a link between developmental speed and physiological stress in an omnivorous insect. *Front. Behav. Neurosci.* **13**, 42 (2019).
51. Farquhar, G. D., von Caemmerer, S. & Berry, J. A. A biochemical model of photosynthetic CO₂ assimilation in leaves of C3 species. *Planta* **149**, 78–90 (1980).
52. Medlyn, B. E. et al. Reconciling the optimal and empirical approaches to modelling stomatal conductance. *Glob. Change Biol.* **17**, 2134–2144 (2011).
53. Gimeno, T. E. et al. Conserved stomatal behavior under elevated CO₂ and varying water availability in a mature woodland. *Funct. Ecol.* **30**, 700–709 (2016).
54. Yang, J. et al. Incorporating non-stomatal limitation improves the performance of leaf and canopy models at high vapor pressure deficit. *Tree Physiol.* **39**, 1961–1974 (2019).
55. Martins, C. S. C. et al. Identifying environmental drivers of greenhouse gas emissions under warming and reduced rainfall in boreal-temperate forests. *Funct. Ecol.* **31**, 2356–2368 (2017).
56. Zhang, X. & Wang, W. The decomposition of fine and coarse roots: their global patterns and controlling factors. *Sci. Rep.* **5**, 9940 (2015).
57. Reich, P. B. et al. Plant diversity enhances ecosystem responses to elevated CO₂ and nitrogen deposition. *Nature* **410**, 809–810 (2001).
58. Gherlenda, A. N., Moore, B. D., Haigh, A. M., Johnson, S. N. & Riegler, M. Insect herbivory in a mature *Eucalyptus* woodland canopy depends on leaf phenology but not CO₂ enrichment. *BMC Ecol.* **16**, 47 (2016).
59. Gherlenda, A. N. et al. Precipitation, not CO₂ enrichment, drives insect herbivore frass deposition and subsequent nutrient dynamics in a mature *Eucalyptus* woodland. *Plant Soil* **399**, 29–39 (2016).
60. Drake, J. E. et al. The partitioning of gross primary production for young *Eucalyptus tereticornis* trees under experimental warming and altered water availability. *New Phytol.* **222**, 1298–1312 (2019).
61. Salomón, R. L., Steppé, K., Crous, K. Y., Noh, N. J. & Ellsworth, D. S. Elevated CO₂ does not affect stem CO₂ efflux nor stem respiration in dry *Eucalyptus* woodland, but it shifts the vertical gradient in xylem CO₂. *Plant Cell Environ.* **42**, 2151–2164 (2019).
62. Raumonen, P. et al. Fast automatic precision tree models from terrestrial laser scanner data. *Remote Sens.* **5**, 491–520 (2013).
63. Calders, K. et al. Nondestructive estimates of above-ground biomass using terrestrial laser scanning. *Methods Ecol. Evol.* **6**, 198–208 (2015).
64. Davidson, E. A., Samanta, S., Caramori, S. S. & Savage, K. The dual Arrhenius and Michaelis-Menten kinetics model for decomposition of soil organic matter at hourly to seasonal time scales. *Glob. Change Biol.* **18**, 371–384 (2012).
65. Guenther, A. B. et al. The Model of Emissions of Gases and Aerosols from Nature version 2.1 (MEGAN2.1): an extended and updated framework for modeling biogenic emissions. *Geosci. Model Dev.* **5**, 1471–1492 (2012).
66. Emmerson, K. M., Palmer, P. I., Thatcher, M., Haverd, V. & Guenther, A. B. Sensitivity of isoprene emissions to drought over south-eastern Australia: integrating models and satellite observations of soil moisture. *Atmos. Environ.* **209**, 112–124 (2019).
67. Kännaste, A., Copolovici, L. & Niinemets, Ü. Gas chromatography mass-spectrometry method for determination of biogenic volatile organic compounds emitted by plants. In *Plant Isoprenoids: Methods And Protocols* (ed. Rodriguez-Concepción, M.) 161–169 (Humana Press, 2014).
68. Tholl, D. et al. Practical approaches to plant volatile analysis. *Plant J.* **45**, 540–560 (2006).
69. Li, T., Holst, T., Michelsen, A. & Rinnan, R. Amplification of plant volatile defense against insect herbivory in a warming Arctic tundra. *Nat. Plants* **5**, 568–574 (2019).
70. Johnsen, L. G., Skou, P. B., Khakimov, B. & Bro, R. Gas chromatography—mass spectrometry data processing made easy. *J. Chromatogr. A* **1503**, 57–64 (2017).
71. Keith, H. et al. Multiple measurements constrain estimates of net carbon exchange by a *Eucalyptus* forest. *Agric. For. Meteorol.* **149**, 535–558 (2009).
72. Bates, D., Machler, M., Bolker, B. M. & Walker, S. C. Fitting linear mixed-effects models using lme4. *J. Stat. Softw.* **67**, 1–48 (2015).
73. R Core Team. *R: A Language And Environment For Statistical Computing* <https://www.R-project.org/> (R Foundation for Statistical Computing, 2018).
74. Ouimet, A. P. et al. Accounting for carbon flux to mycorrhizal fungi may resolve discrepancies in forest carbon budgets. *Ecosystems* <https://doi.org/10.1007/s10021-019-00440-3> (2019).
75. Harris, I., Jones, P. D., Osborn, T. J. & Lister, D. H. Updated high-resolution grids of monthly climatic observations—the CRU TS3.10 dataset. *Int. J. Climatol.* **34**, 623–642 (2014).
76. Olson, D. M. et al. Terrestrial ecoregions of the world: a new map of life on Earth. *Bioscience* **51**, 933–938 (2001).
77. Jiang, M., Felzer, B. S., Nielsen, U. N. & Medlyn, B. E. Biome-specific climatic space defined by temperature and precipitation predictability. *Glob. Ecol. Biogeogr.* **26**, 1270–1282 (2017).
78. Scarscia-Mugnoza, G. et al. Response to elevated CO₂ of a short rotation, multispecies Poplar plantation: the POPFACE/EUROFACE experiment. In *Managed Ecosystems and CO₂* (eds. Nösberger, J. et al.) 173–195 (Springer, 2006).
79. Linder, S. NPP Boreal Forest: Flakaliden, Sweden, 1986–1996, R1. Dataset at <https://doi.org/10.3334/ORNLDAC/201> (Oak Ridge National Laboratory Distributed Active Archive Center, 2013).
80. Anderson-Teixeira, K. J. et al. ForC: a global database of forest carbon stock and fluxes. *Ecology* **99**, 1507 (2018).
81. Shangguan, W., Dai, Y., Duan, Q., Liu, B. & Yuan, H. A global soil data set for Earth system modelling. *J. Adv. Model. Earth Syst.* **6**, 249–263 (2014).
82. Yang, X., Post, W.M., Thornton, P.E. and Jain, A. *Global gridded soil phosphorus distribution maps at 0.5-degree resolution*. Dataset at <https://doi.org/10.3334/ORNLDAC/1223> (Oak Ridge National Laboratory Distributed Active Archive Center, 2014).

Acknowledgements EucFACE was built as an initiative of the Australian Government as part of the Nation-building Economic Stimulus Package, and is supported by the Australian Commonwealth in collaboration with Western Sydney University. We acknowledge technical support by V. Kumar, C. McNamara and S. Wohl, and the team who assisted with data collection. This work was partially supported by the following grants from the Australian Research Council (ARC): DP130102501 (to J.R.P. and I.C.A.), DP170104634 (to B.K.S. and P.B.R.), DP170102766 (to E.P. and M.G.T.), DP110105102 and DP160102452 (to D.S.E.). M.G.D.K. acknowledges funding from the ARC Centre of Excellence for Climate Extremes (CE170100023), the ARC Discovery Grant (DP190101823) and support from the NSW Research Attraction and Acceleration Program. R.L.S. received funding from Research Foundation Flanders and the European Union's Horizon 2020 research and innovation programme under the Marie Skłodowska-Curie grant agreement number 665501. R.O.-H. is financially supported by a Ramón y Cajal Fellowship from MICIU (RYC-2017-22032). E.H.J.N. and B.M.D.S. received funding from the VILLUM Center for Plant Plasticity (VKRO23054), the VILLUM Young Investigator Program fellowship (VKRO13167), and a Danish Independent Research Council Sapere Aude Research Talent Post-Doctoral Stipend (6111-00379B). Ü.N. and A.K. were supported by the European Commission through the European Regional Fund (Center of Excellence EcolChange). S.Z. was supported by the European Research Council under the European Union's Horizon 2020 research and innovation programme (grant agreement number 647204, QUINCY).

Author contributions M.J., B.E.M., R.A.D. and J.E.D. designed the synthesis, compiled the data and performed the analyses. M.J., B.E.M., J.E.D., R.A.D., I.C.A., C.V.M.B., M.M.B., Y.C., L.C.-G., L.C., K.Y.C., B.M.D.S., S.L.F., A.N.G., T.E.G., S.H., S.N.J., A.K., C.A.M., K.M., B.D.M., L.N., E.H.J.N., Ü.N.N., Ü.N., N.J.N., R.O.-H., V.S.P., E.P., J. Pihlblad, J. Pineiro, J.R.P., S.A.P., P.B.R., A.A.R., M.R., R.R., P.D.R., R.L.S., B.K.S., B.M.G.T., J.K.M.W., A.W.-K., J.Y. and D.S.E. collected data and contributed to data analyses. M.J. performed data assimilation analysis, with contributions from M.G.D.K. and B.E.M. J.Y. and B.E.M. performed the MAESPA model simulations, with contributions from M.G.D.K. and R.A.D. J.E.D. and A.A.R. performed soil respiration gap-filling and modelling. K.M.E. performed the MEGAN model simulation. M.J. and L.C.-G. conceptualized Fig. 1, and L.C.-G. implemented the graphic design and hand-drew all the vectors in the figure. M.J. wrote the initial manuscript, with substantial input from B.E.M., J.E.D., B.S., P.B.R., S.Z., M.G.D.K., M.G.T. and D.S.E. All authors edited and approved the manuscript.

Competing interests The authors declare no competing interests.

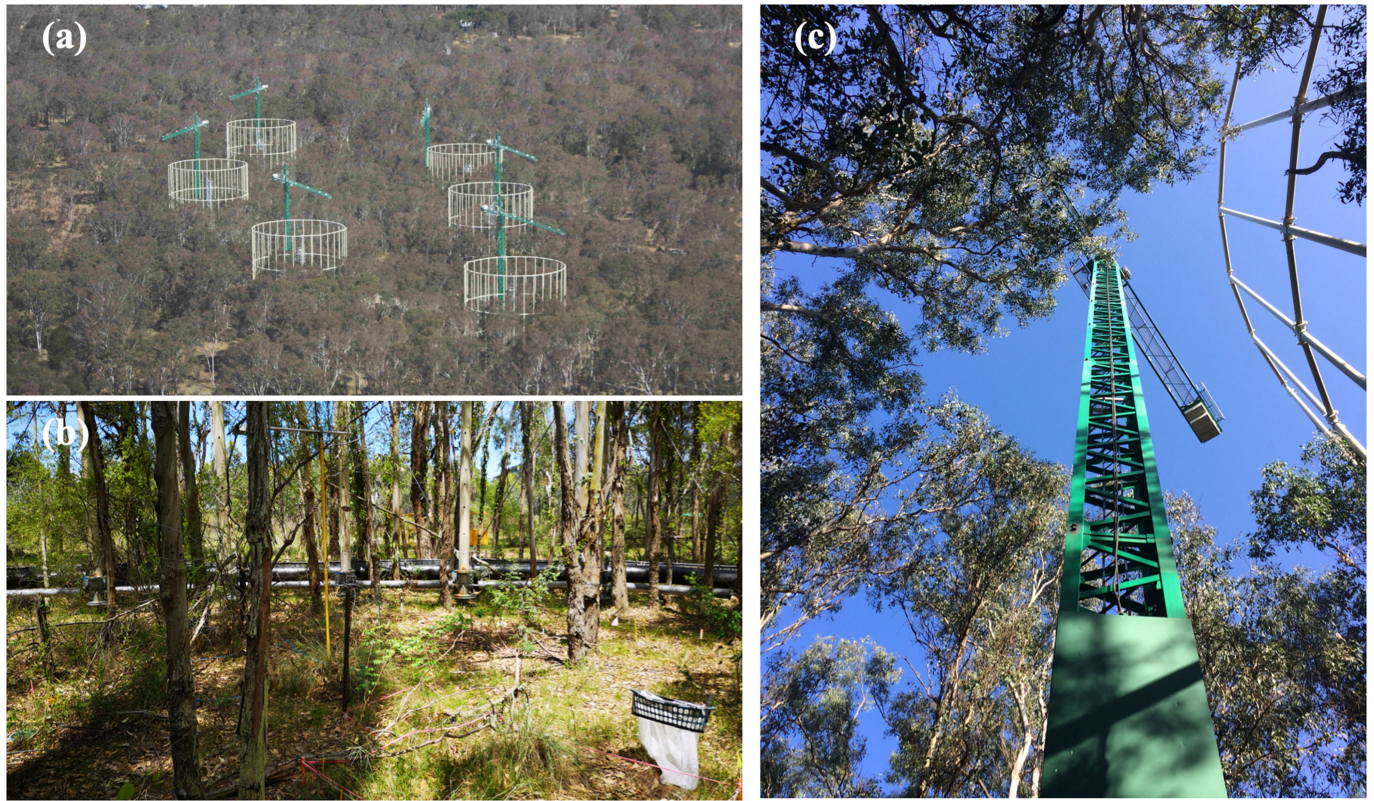
Additional information

Supplementary information is available for this paper at <https://doi.org/10.1038/s41586-020-2128-9>.

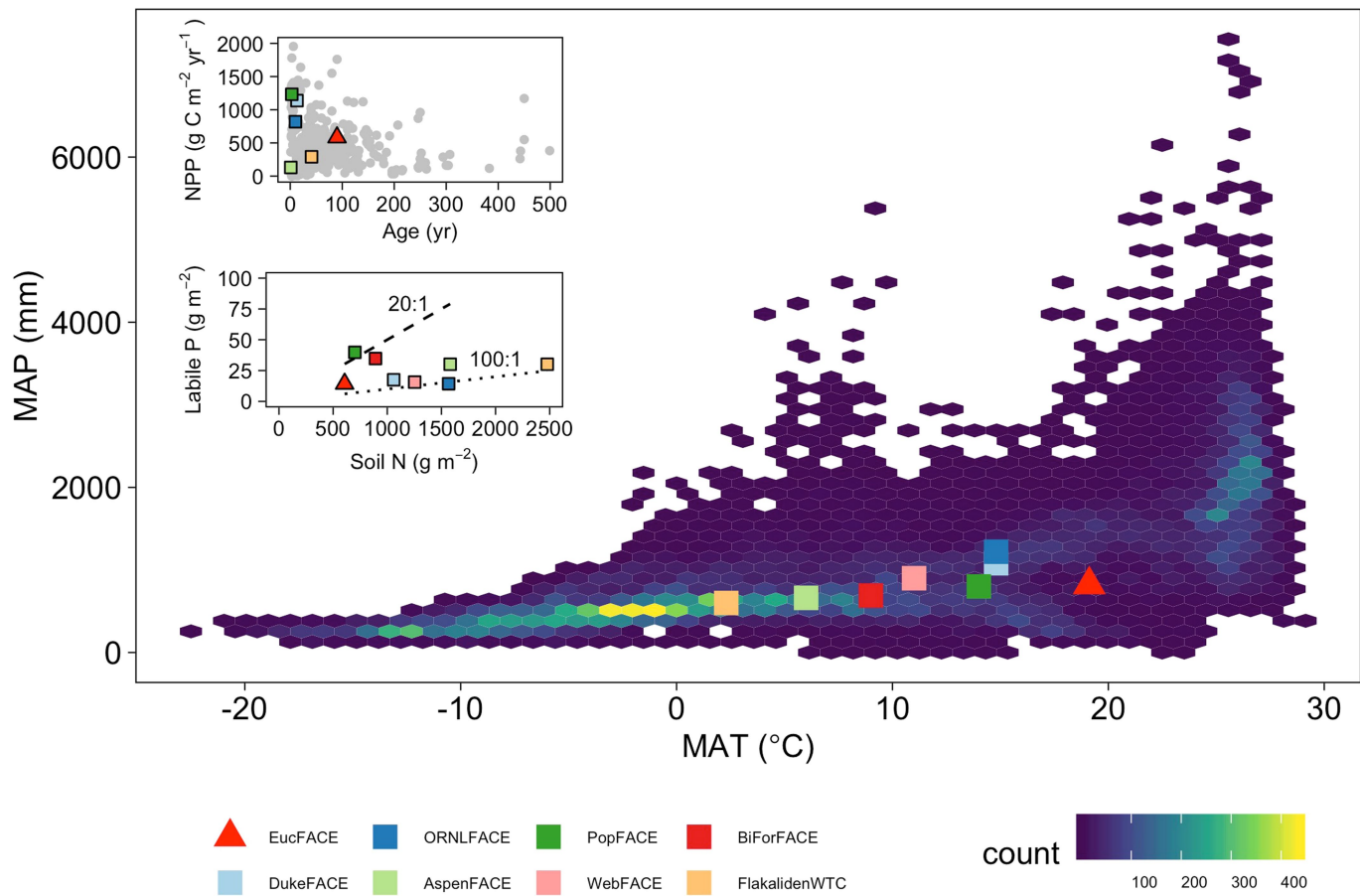
Correspondence and requests for materials should be addressed to M.J. or B.E.M.

Peer review information *Nature* thanks Kirsti Ashworth, Benjamin Bond-Lamberty, Yiqi Luo and Andrew Richardson for their contribution to the peer review of this work.

Reprints and permissions information is available at <http://www.nature.com/reprints>.

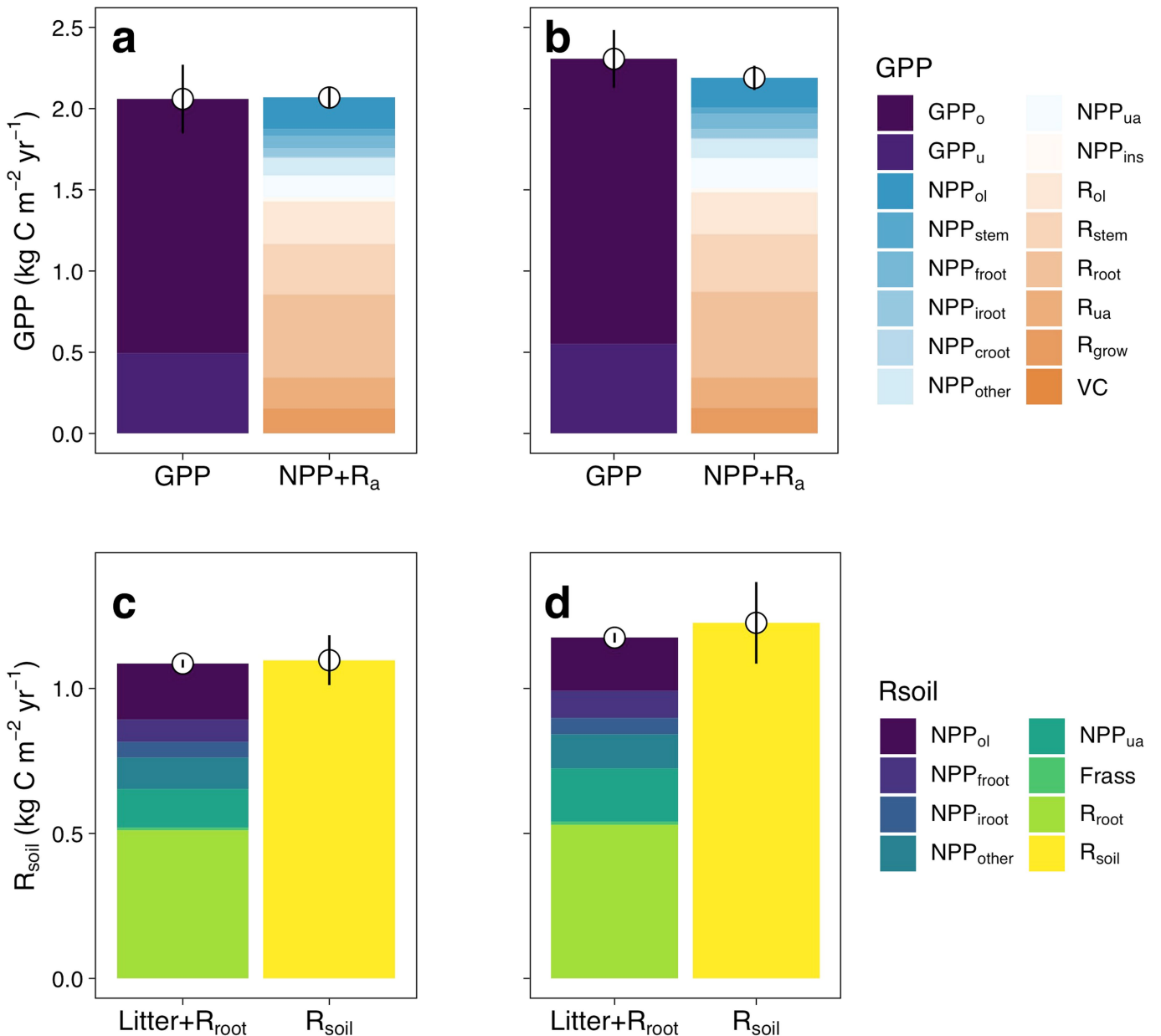


Extended Data Fig. 1 | The EucFACE experiment facility. **a**, View of the forest and facility from above (photograph taken by D.S.E.). **b**, View of the understorey vegetation and infrastructure inside a plot (photograph taken by M.J.). **c**, View from below of the canopy structure and the crane (photograph taken by M.J.).



Extended Data Fig. 2 | Mean annual temperature (MAT) and mean annual precipitation (MAP) for major forest biomes and a selected list of tree-based elevated CO₂ experiments. Gridded temperature and precipitation data were obtained from the Climate Research Unit monthly dataset at 0.5-degree resolution⁷⁵. Global biome boundaries and definitions were taken from ref.⁷⁶ and were spatially aggregated onto the Climate Research Unit resolution, following ref.⁷⁷. Only forest biomes were included here, including: tropical and subtropical moist broadleaf forests; tropical and subtropical dry broadleaf forests; tropical and subtropical coniferous forest; temperate broadleaf and mixed forests; temperate coniferous forests; boreal forests/taiga; and Mediterranean forests, woodlands, and scrub. The list of elevated CO₂ experiments includes seven FACE experiments and a Whole-Tree Chamber

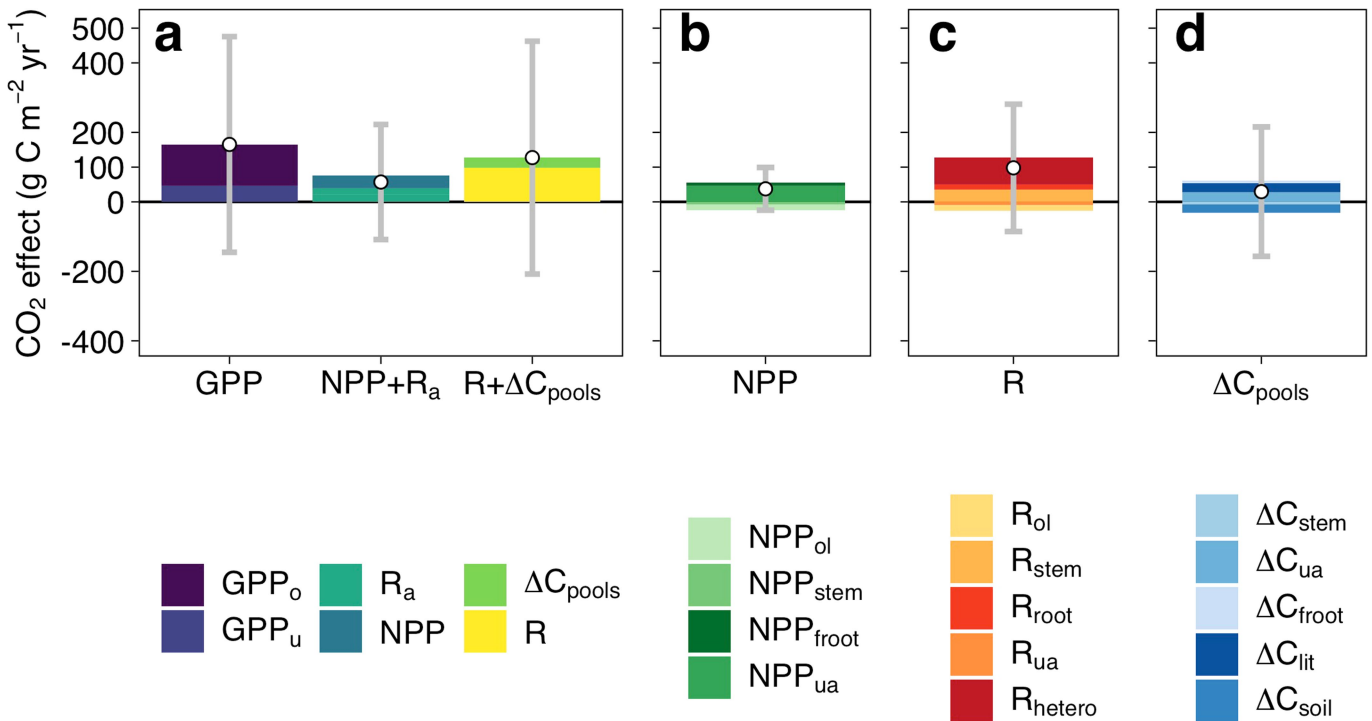
(WTC) experiment, namely: EucFACE, DukeFACE, ORNLFACE, AspenFACE, PopFACE, WebFACE, BiForFACE and FlakalidenWTC. The site-specific climate, tree age and net primary production (NPP) under ambient CO₂ treatment were collected from refs.^{3,9–11,78,79}. The top inset compares global forest NPP against standing age using data collected from ref.⁸⁰. We included data with forest age <500 years, and the NPP reported in ref.⁸⁰ includes both overstorey and understorey. The bottom inset compares soil total nitrogen and labile phosphorus across the eCO₂ experiments. Soil total nitrogen was extracted from ref.⁸¹ using the spatial coordinates of each experiment, while soil labile phosphorus was spatially extracted from ref.⁸². The two dotted lines indicate N:P ratios of 20:1 and 100:1, respectively. The count in the colour scale refers to the number of grids that fall within each climate space.



Extended Data Fig. 3 | Estimates of GPP (a, b) and soil respiration (R_{soil}) (c, d) based on different methods for both ambient (a, c) and elevated (b, d) CO_2 treatment at EucFACE. For estimates of GPP, we compared the model simulated total GPP of overstorey and understorey (GPP_o and GPP_u , respectively), with the sum of data-driven estimates of net primary production (NPP) and autotrophic respiration (R_a), which include NPP of overstorey leaf (NPP_{ol}), stem (NPP_{stem}), fine root (NPP_{froot}), intermediate root (NPP_{iroot}), coarse root (NPP_{croot}), twigs, barks and seeds (NPP_{other}), understorey aboveground (NPP_{ua}), leaf consumption by insects (NPP_{ins}), and respiratory fluxes of overstorey leaf (R_{ol}), stem (R_{stem}), root (R_{root}), understorey aboveground (R_{ua}), growth (R_{grow}), and volatile carbon emission (VC). For estimates of R_{soil} , we compared direct estimates of R_{soil} scaled up from soil chamber measurements,

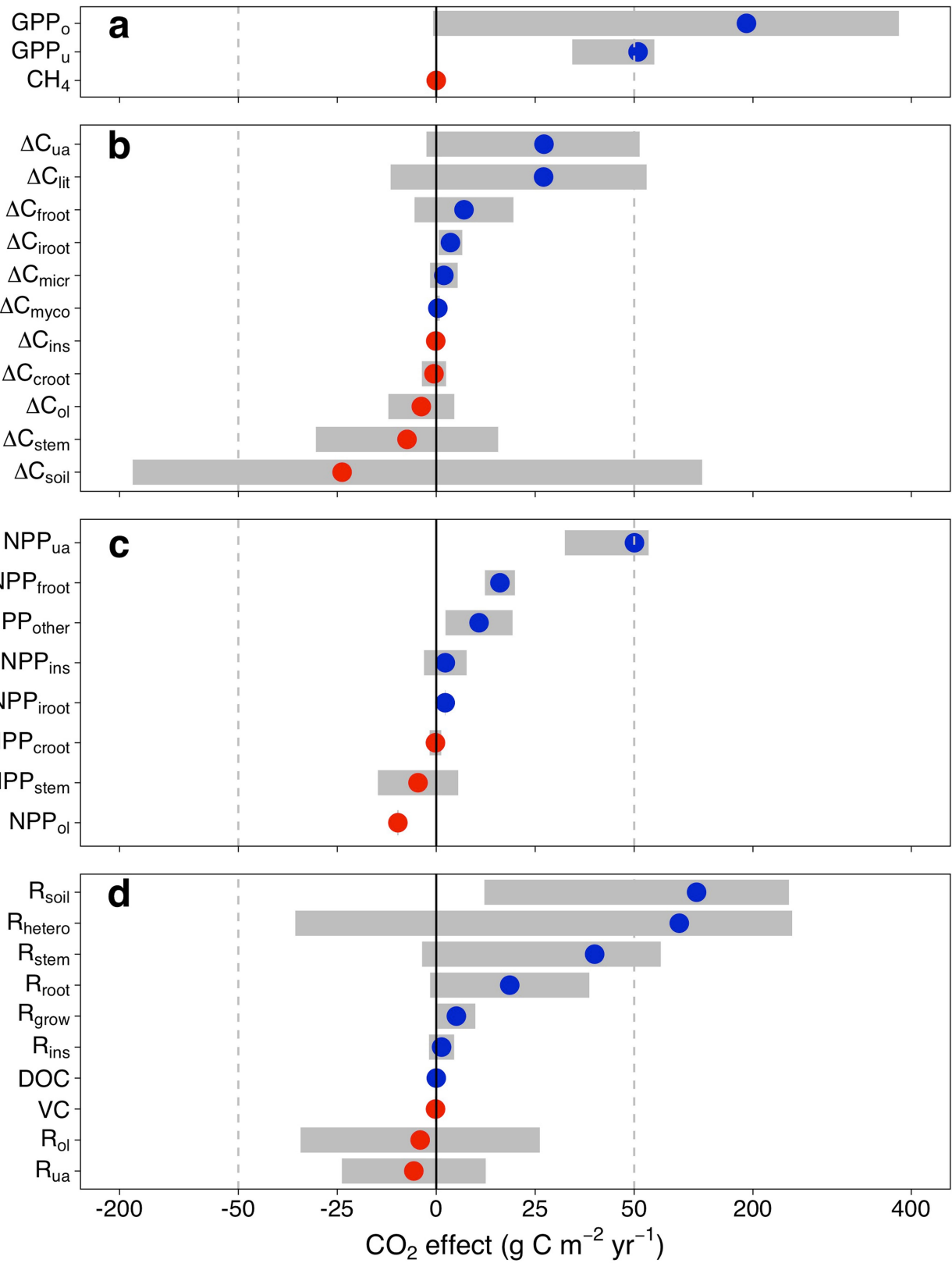
with the sum of litterfall and independent estimates of root respiration ($Litter + R_{root}$), assuming no net change in soil carbon stock over time. Here litterfall was inferred from the NPP of overstorey leaf (NPP_{ol}), fine root (NPP_{froot}), intermediate root (NPP_{iroot}), twigs, barks and seeds (NPP_{other}), understorey aboveground (NPP_{ua}), and frass production (Frass). These evaluations provide independent mass balance checks of the estimated ecosystem carbon budget. Each colour represents a flux variable. Each point and vertical line represent treatment mean and standard deviation, respectively, based on plot-level estimates of the aggregated flux ($n = 3$). Values were normalized by a linear mixed model with pre-treatment LAI as a covariate to account for pre-existing differences.

Article



Extended Data Fig. 4 | The fate of additional carbon fixed under elevated CO₂ (eCO₂) in a mature forest ecosystem (non-normalized analysis case). **a**, GPP represents the total eCO₂ induced increase in GPP_o and GPP_u, respectively, NPP + R_a represents the sum of net primary production and autotrophic respiration eCO₂ response, and R + ΔC_{pool} represents the sum of ecosystem respiration and carbon storage eCO₂ response. **b**, The relative contributions of individual NPP fluxes to the aggregated NPP response to eCO₂, including overstorey leaf (NPP_{ol}), stem (NPP_{stem}), fine root (NPP_{froot}) and understorey aboveground (NPP_{ua}). **c**, The relative contributions of individual respiratory fluxes to the

aggregated R response to eCO₂, including overstorey leaf (R_{ol}), stem (R_{stem}), root (R_{root}), understorey aboveground (R_{ua}), and heterotroph (R_{hetero}). **d**, The relative contributions of individual change in carbon storage to the aggregated ΔC_{pool} response to eCO₂, including stem (ΔC_{stem}), fine root (ΔC_{froot}), leaf litter (ΔC_{lit}), understorey aboveground (ΔC_{ua}), and soil (ΔC_{soil}). Variables with an average CO₂ effect of <5 g C m⁻² yr⁻¹ were excluded from the figure for better visual clarification. Each colour represents a flux variable, each point indicates the net sum of all variables for a column, and the grey error bar represents the plot-level standard deviation ($n=3$) of the estimated column sum.

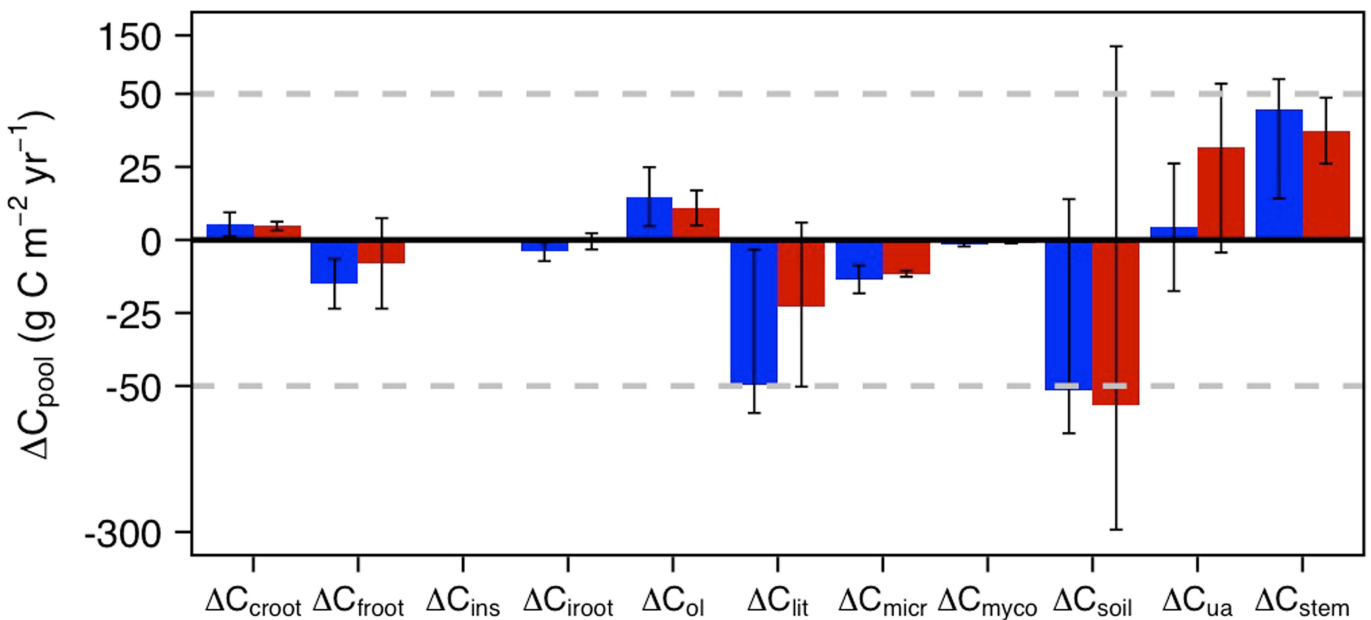


Extended Data Fig. 5 | See next page for caption.

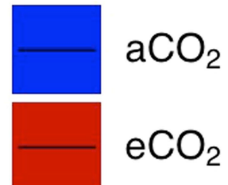
Article

Extended Data Fig. 5 | CO₂ treatment effect for all ecosystem fluxes at EucFACE. **a**, The CO₂ response of gross ecosystem carbon uptake, including GPP_o and GPP_u, and soil methane uptake (CH₄). **b**, The eCO₂ response of annual incremental change in carbon pool (ΔC_{pool}), including overstorey leaf (ΔC_{ol}), stem (ΔC_{stem}), coarse root (ΔC_{croot}), fine root (ΔC_{froot}), intermediate root (ΔC_{iroot}), understorey aboveground (ΔC_{ua}), leaf litter (ΔC_{lit}), soil (ΔC_{soil}), microbe (ΔC_{micr}), aboveground insect (ΔC_{ins}), and mycorrhizae (ΔC_{myco}). **c**, The eCO₂ response of NPP, including overstorey leaf (NPP_{ol}), stem (NPP_{stem}), coarse root (NPP_{croot}), fine root (NPP_{froot}), intermediate root (NPP_{iroot}), understorey aboveground (NPP_{ua}),

twigs, barks and seeds (NPP_{other}), and leaf insect consumption (NPP_{ins}). **d**, The eCO₂ response of ecosystem R and other outgoing fluxes, including respiration fluxes of overstorey leaf (R_{ol}), stem (R_{stem}), root (R_{root}), understorey aboveground (R_{ua}), growth (R_{grow}), insect (R_{ins}), heterotroph (R_{hetero}), and soil (R_{soil}), and volatile carbon emission (VC) and DOC leaching. Dots and grey bars represent means and standard deviations of the CO₂ treatment difference, predicted by a linear mixed model with plot-specific pre-treatment LAI as a covariate. Red dots indicate negative means and blue dots indicate positive means. Dashed lines indicate change of scale along the x-axis.

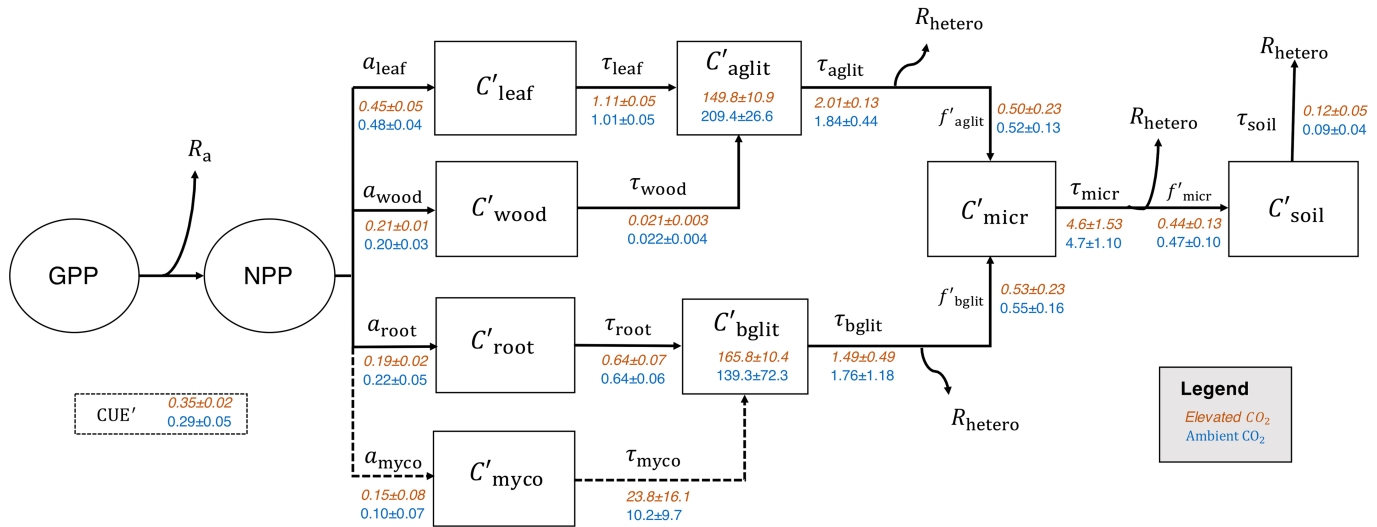


Treatment



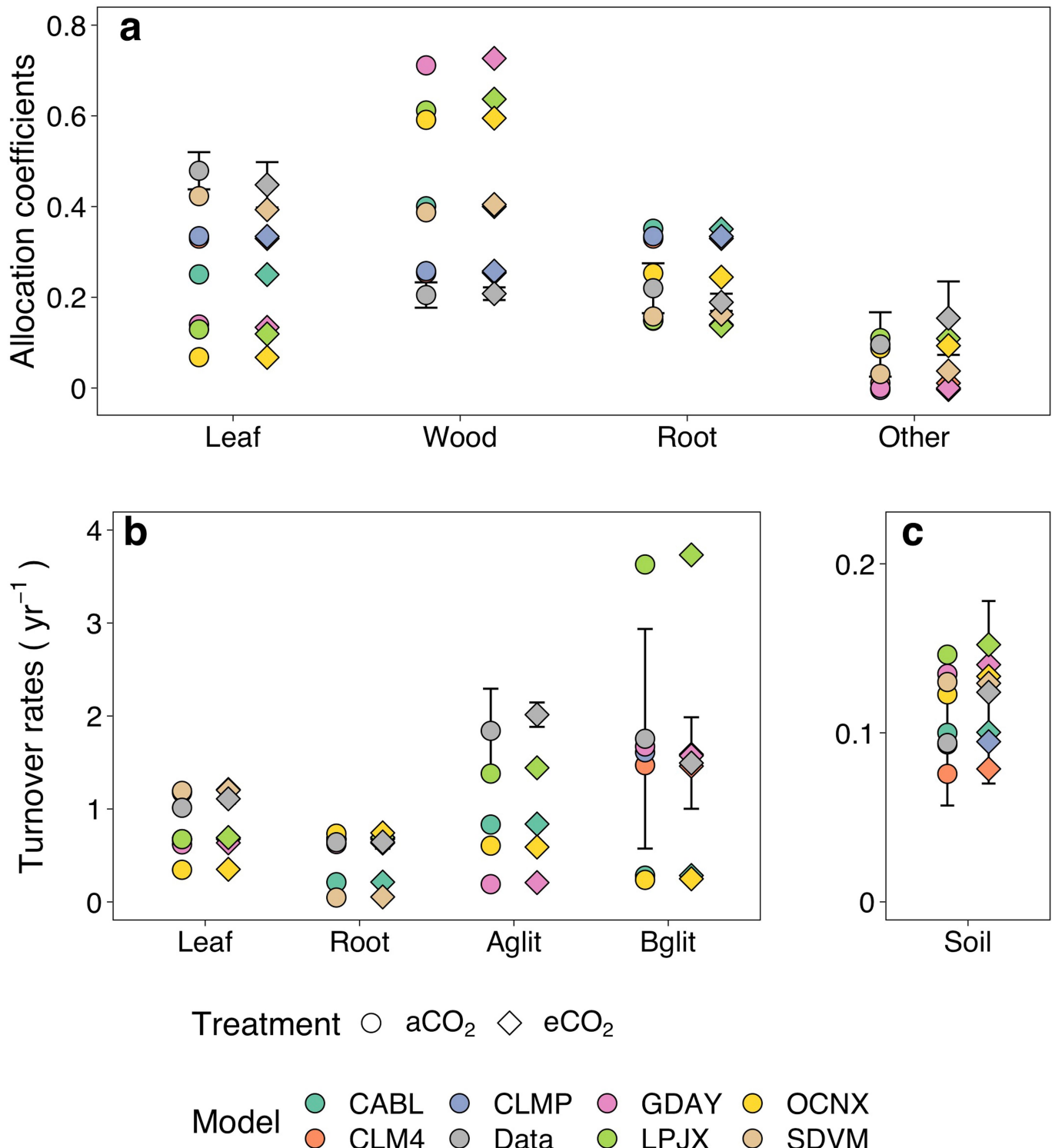
Extended Data Fig. 6 | Estimates of incremental change in carbon pool averaged over the experimental period under ambient (aCO₂) and elevated CO₂ (eCO₂) treatment effect at EucFACE (ΔC_{pool}). The ΔC_{pool} variables are overstorey leaf (ΔC_{ol}), stem (ΔC_{stem}), coarse root (ΔC_{croot}), fine root (ΔC_{froot}), intermediate root (ΔC_{iroot}), understorey aboveground (ΔC_{ua}), leaf litter (ΔC_{lit}),

soil (ΔC_{soil}), microbe (ΔC_{micr}), aboveground insect (ΔC_{ins}), and mycorrhizae (ΔC_{myco}). Each coloured bar and black line (error bar) represents the mean and standard deviation for each treatment, with blue representing aCO₂ and red representing eCO₂ treatment. Dashed lines indicate change of scale along the x axis.



Extended Data Fig. 7 | Fitted carbon cycle parameters to trace the fate of the additional carbon under elevated CO₂ at EucFACE. Parameters were estimated by MCMC fitting algorithm, assuming a simplified carbon cycle framework based on data collected from EucFACE. Details of the MCMC approach can be found in the Methods. Plot-level GPP, autotrophic respiration (R_a), heterotrophic respiration (R_{hetero}), carbon pools of leaf (C'_{leaf}), wood (C'_{wood}), root (C'_{root}), mycorrhizae (C'_{myco}), microbe (C'_{micr}), and soil (C'_{soil}), and the corresponding change in pools were used to constrain the model fitting. NPP

was derived as the difference of GPP and R_a . Carbon use efficiency (CUE') was calculated as NPP/GPP; it differs from the value given in the main text owing to the contribution of NPP allocated to mycorrhizae (NPP_{myco}). We fitted two carbon pools (C'_{aglit} and C'_{bglit}), four allocation coefficients (a_{leaf} , a_{wood} , a_{root} and a_{myco}), six turnover rates (τ_{leaf} , τ_{root} , τ_{myco} , τ_{bglit} , τ_{micr} and τ_{soil}), and three fractional coefficients (f'_{aglit} , f'_{bglit} and f'_{micr}) using the MCMC algorithm. The fractional coefficients indicate the fraction of carbon leaving one pool that enters the subsequent pool, with the remainder respired as R_{hetero} .



Extended Data Fig. 8 | Data–model intercomparison of some key carbon cycle parameters, under ambient (aCO₂) and elevated CO₂ (eCO₂). Parameters include: **a**, allocation coefficients to leaf, wood, root and other; **b**, turnover rates of leaf, root, aboveground litter (Aglit), belowground litter (Bglit); and **c**, turnover rate of soil. Models include: Community Atmosphere Biosphere Land Exchange (CABL), Community Land Model 4 (CLM4), Community Land Model with a phosphorus component (CLMP), Generic Decomposition And Yield (GDAY), Lund-Potsdam-Jena General Ecosystem Simulator (LPJX), Orchidee-

C-N (OCNX) and Sheffield Dynamic Global Vegetation Model (SDVM). The model output was generated as part of the model ensemble predictions made in advance of the experiment reported in ref.¹⁷ for EucFACE. Database uncertainties were estimated using the MCMC data assimilation algorithm, with error bars indicating one standard deviation. Allocation to ‘Other’ in the data refers to the allocation to mycorrhizal production, whereas in some models it refers to the allocation to reproductive carbon pool.